ABSTRACT

DEPARTMENT OF CHEMISTRY

LONDON, LAURISA A. B.S. CLARK ATLANTA UNIVERSITY, 2008

THE EFFECT OF STEREOCHEMISTRY AND CONFORMATION ON NANOCOMPOSITE FORMATION

Committee Chair: Ishrat Khan, Ph.D.

Dissertation dated December 2013

Through the dispersion of nanofillers into polymer matrices, high-performance lightweight composites were heralded as the new class of materials with multifunctional properties. Although the design and fabrication of nanocomposites with flexible and controlled properties are an ongoing challenge, these materials have potential use in microoptics, electronics and solar cells. Nanofillers enhanced performance is achieved by their inherent optical, electrical and magnetic properties. These properties become more evident with decreasing particle size, thus leading to an increase in the surface/volume ratio. The filler's properties at a nano-scale are substantially different compared to that of their bulk counterparts. Therefore, the smaller a particle is, the greater its role in influencing the interfacial and physical properties as well as agglomeration behavior of composites. While much is known about polymer material preparation, not much is

understood on how to tailor polymer structures to control self-assembly. With the pioneering of new technologies there is still a great desire to fully understand the mechanism by which one-dimensional nanostructures change the structural and thermal properties of host materials. In order to fabricate high performance devices, it is crucial to achieve effective control over the self-assembly of copolymers and their fillers. Understanding the process, phase transitions, and surface effects in which particle-polymer interact is important in developing a broader perspective on composite formation.

THE EFFECT OF STEREOCHEMISTRY AND CONFORMATION ON NANOCOMPOSITE FORMATION

A DISSERTATION

SUBMITTED TO THE FACULTY OF CLARK ATLANTA UNIVERSITY

IN PARTIAL FULFILLMENT OF THE REQUIREMENTS FOR

THE DEGREE OF DOCTOR OF PHILOSOPHY

BY LAURISA ANN LONDON

DEPARTMENT OF CHEMISTRY

ATLANTA, GEORGIA

MAY 2014

ACKNOWLEDGEMENTS

I would like to thank my advisor Dr. Ishrat Khan for his guidance and support, while pursuing my degree. His wealth of knowledge has been invaluable to my journey through graduate school. I am thankful for all of the opportunities he initiated, such as, presenting at conferences, international travel, international and domestic collaborations internships and journal publishing.

I would also like to thank Pat Marsteller and Jordan Rose at Emory College Center for Science Education for the NSF PRISM fellowship.

Special thanks to Dr. James Reed, Dr. Myron Williams, Dr. Issifu Harruna, Ms. Muzar Jah, Dr. Cass Parker, Dr. Biswajit Sannigrahi, Dr. Conrad Ingram, Dr. Michelle Gaines, Dr. Eric Mintz and Dr. James Bu for providing equipment, materials, resources, valuable conversations, collaborations and serving on my thesis committee.

Finally, I am grateful for my family and friends for their love, support, prayers and belief in me. I am especially thankful to my mom, Eulalie London and dad, Leland A. London for instilling good ethics and morals in me. Also, I would like to thank Tim Dawodu for all of his support.

TABLE OF CONTENTS

LIST OF FIGURES

CHAPTER 1
THE SUPRAMOLECULAR ASSEMBLY OF INORGANIC NANOPARTICLES ON BLOCK COPOLYMERIC SYSTEMS

LIST OF TABLES

LIST OF ABBREVIATIONS

GONR	Graphene Oxide Nanoribbons
SWNT	Single-Walled Nanotubes
FGS	Functionalized Graphene Sheets
EG	Expanded Graphite
DSC	Differential Scanning Calorimetry
FTIR	Fourier Transform Infrared spectroscopy
k	10^3
M_n	Number average molecular weight
mL	milliliter
Mw	Molecular weight
NaOH	Sodium Hydroxide
nm	Nanometers
NMR	Nuclear Magnetic Resonance spectroscopy
PEG	Polyethylene glycol
PS	Polystyrene
TGA	Thermogravimentric analysis
THF	Tetrahydrofuran
TMS	Tetramethylsilane
^1H	Proton
DMF	Dimethylformamide

CHAPTER 1

THE SUPRAMOLECULAR ASSEMBLY OF INORGANIC NANOPARTICLES ON BLOCK COPOLYMERIC SYSTEMS

1.1 Introduction

In the 1960s a new paradigm for materials was created; polymer-based composites were proclaimed as ideal materials because the ease of processibility was coupled with dramatically increasing the thermal, mechanical and electrical properties of the host polymer at low filler loadings ($< 2vol\%$). Fabrication of nanocomposite materials is accomplished by the use of fillers such as graphene-oxide nanoribbons (GONRs), carbon nanotubes (CNTs), expanded graphite (EG) and functionalized graphene sheets (FGS) to name a few.[1] The fillers' size, shape, surface area, and chemical nature modify the host polymers' electrical, mechanical, thermal, and barrier properties at low filler content. Functionalized nanostructures are instrumental in the development of strong, durable and high-performance lightweight composites that are capable of being tailored to individual applications, e.g., microoptics, electronics and energy conversion or storage.[2]

Before discussing in detail the various preparation methods for nanocomposite, one has to consider the success in using filler materials that are small in size. A nanoparticle is defined as a particle with diameters well below the micron dimension (below 100 nm). Nanofillers enhanced performance is achieved by their inherent optical,

electrical and magnetic properties. These properties become more evident with decreasing particle size, because of an increase in the surface/volume ratio. In this context, a 5 nm particle consisting of 1000 atoms possesses 40% of their atoms on the surface. In contrast, a 200 nm particle contains 200 million atoms, but a mere 2% of the atoms are located on the surface. Therefore, the smaller a particle is, the greater its role in influencing the interfacial and physical properties as well as agglomeration behavior. These properties at the nanoscale may be different compared to their bulk counterparts, thus the effects are vital, as they will strongly impact the desired properties of the individual applications.

Although physical microphase separation behavior of nanocomposites have been reported more extensively, there is little to no knowledge on the effect polymers have on the self-assembly with nanoparticles. Fundamentally, molecular assembly is omnipresent in nature and in daily life. In nature, the protein collagen found in tendons and ligaments consists of three helices that entwine or self-assembles into a super helix playing a supreme role in both its strength and functions. Soap in water creates soap micelles which originates from the self-assembly of small molecule surfactants. The self-assembly of small molecule amphiphiles have been studied as early as 1976.[1,2] However, in both solution and bulk, there is a great challenge that requires an interdisciplinary approach including diverse backgrounds of disciplines, and materials systems to develop an understanding of the fundamental phase behavior and self-assembly of these systems. The incorporation of nanotechnology into consumer products is a growing trend. Samsung Corporation introduced the use of silver nanoparticles in their household

appliances, such as, washing machines and refrigerators to minimize odors and eliminate bacteria. There is still a great desire to fully understand the mechanism in which one-dimensional nanostructures change the mechanical and thermal properties of polymers. In particular, we still need to understand many of the requirements necessary to exploit non-covalent interactions to design well-controlled sophisticated higher-level structures.

Various nanostructures have been prepared through self-assembly including one-dimensional (1D) nanofibers and nanotubes as well as two-dimensional (2D) nanoribbons and nanosheets, while three-dimensional nanoparticles are illustrated as nanoporous materials.[3] Nanofibers exhibit special properties mainly due to their extremely high surface to volume ratio compared to that of conventional nonwovens. One-dimensional nanotubes are excellent candidates for polymer blends due to their high mechanical strength, high electrical and thermal conductivity, as well as their unique optical and electronic properties.[4] Interestingly, block copolymers have been identified as ideal candidates for directing the assembly of nanoparticles into ordered mesostructures.[5,6] π-π Stacking usually dominates the self-assembly of these nanostructures with conjugated backbones because of the delocalized π-electrons. Understanding the process, phase transitions, and surface effects in which particle-polymer interact is important in understanding how to improve functional nanocomposites.

Studies focused on efficient charge separation and good charge transport properties lead to the development of highly sensitive and fast responsive sensors.[7-9] The

upshot of such studies is the eventual fabrication of novel therapeutic tools and agents for biodiagnostics. The preparation and evaluation of functional nanofibers capable of selectively interacting with biomolecules were undertaken for the eventual development of biosensors. This dissertation reports on the self-assembly behavior of polymers in the presence of nanoparticles; for the development of well-defined materials and devices with controlled structures and functions.

1.2 Nanostructures

New opportunities for the improvement of novel nanosystems and nanomaterials are made possible through the development of new theoretical and experimental techniques. A study that demonstrates new physical and chemical properties at an intermediate level between the molecular and microcrystalline world furthers the development of novel materials with distinct optical, magnetic and photonic capabilities. Nanocomposites are hybrid materials based on a variety of components spatially organized at both the molecular and nanoscale level where at least one component has nanometric dimensions.

Biological systems have processes that function on both a nano and micro scale level. The lotus and water lily leaves have an anti-adherent property that prevents water from sticking to their surfaces and ultimately rolling off due to gravity. On this nanoscale level there is a certain surface roughness derived from peculiar nanostructures made from long hydrocarbon chains. Findings from such investigative studies could lead to the eventual development of auto-cleaning surfaces for the use in a variety of applications.

There are other natural organic nanostructured materials to name a few, stratified shells of $CaCO_3$ and ornamented cytoskeleton of marine unicellular organism known as diatoms (Figure 1.1), *Mexican Cymbella*. A diatom made of SiO_2 has a structural hierarchical assembly with silica frustrules sculpted in the nanometer range of ordered macropores and mesopores.[1] The pharmaceutical and biomedical industries have interests in producing such supramolecular constructions to fabricate artificial devices capable of imitating complex processes found in nature.[2] These investigative studies have led to the creation of nanocapsules, which mimicked the properties found in liposomes. Nanocapsules assist in the analysis of tissues and organs as they are used as drug delivery vehicles that are capable of selectively releasing drugs on cue with the stimulation of magnetic or fluorescent nanoparticles (NP).

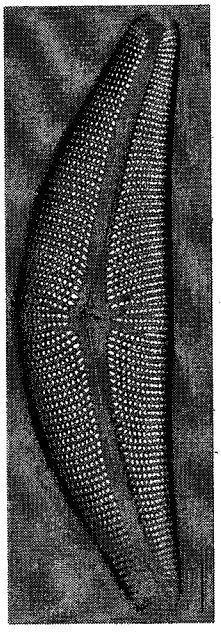

Figure 1.1. Image of crystalline sediment in fossil from reference 43.

Faraday's early experiments on the synthesis and optical behavior of gold nanoparticles lead to the richness of scientific literatures on nontoxic nanoparticles (NPs) found today. The exploitation of nanoparticle excitation spearheaded the development of surface plasmon resonance (SPR) devices. Coupling between plasmon modes within a particle allows a change from visible to near-infrared (NIR) optical resonances. Metal nanoparticle resonances of surface plasmons are governed by the size and shape of nanoparticles. With their optical and magnetic properties, metal particles have been used both as optical bioprobes and in antimicrobial applications. Nanoparticles have a myriad of applications and this translates into our desire to better and more accurately characterize these particles. Nanocrystal formation and characterization have been broadly investigated over the last several years. Some techniques used for NP synthesis include: conventional chemical reduction, heat treatment, microwave irradiation, sonochemical, photolytical, and seeding growth approachs.[3] Nanoparticle properties, such as, stability and particle size strongly rely on the methodology and parameters employed during synthesis.

The surface to volume ratio of nanoparticles compared to that of bulk is significantly higher. Hence; nanocrystalline solid properties are based mainly on surface chemistry. Surface modification of NPs has been used to bind organic compounds such as surfactants or polymers, as well as, to grow distinct inorganic phases using SiO_2 or ZnO, resulting in the assembly of a homogeneous shell around the particle's core (Figure 1.2). Reasons for such common practices are to avoid agglomeration or degradation, to optimization of their surface dependent properties and to improve interaction between the

NPs and their environments. In a biological context, toxic metal particles such as Ti and Ni pose a number of challenges because of their inherent chemical instability. To overcome these pitfalls, polymer nanocomposites are used, provided that the NPs are completely trapped within the polymer matrix, while preserving their functionalities.

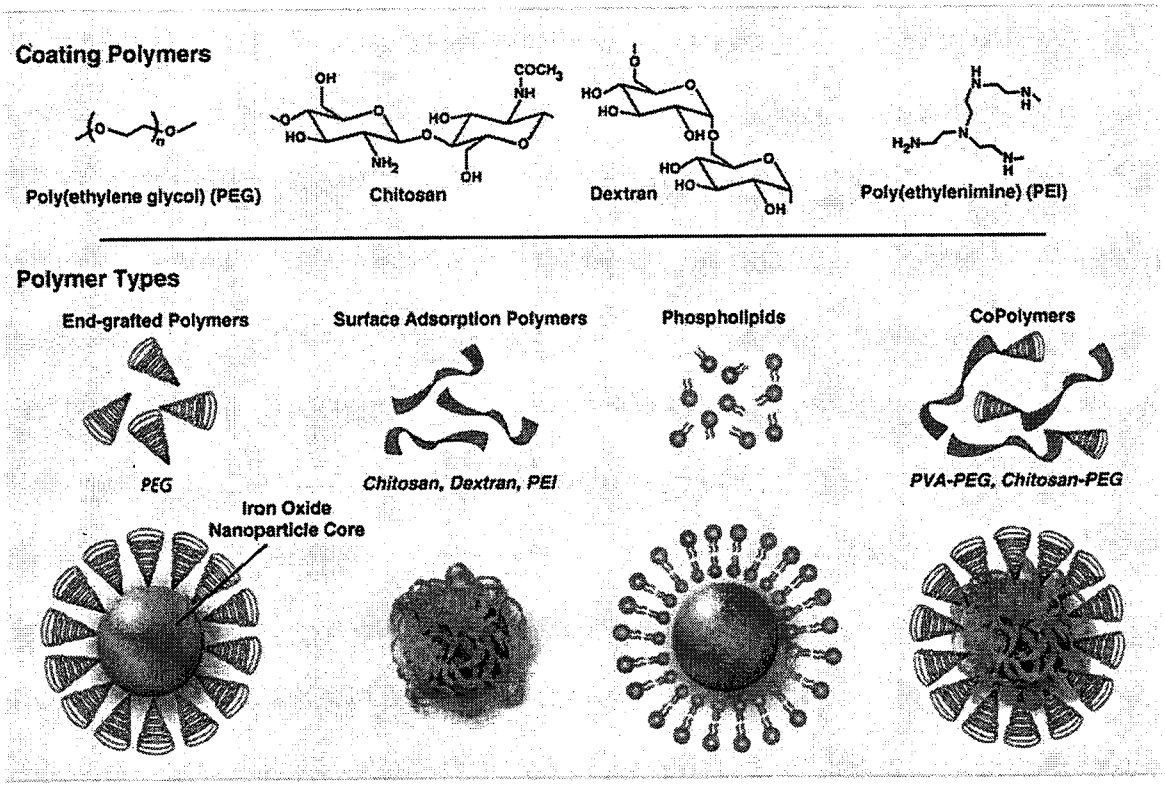

Figure 1.2. Scheme of different nanoparticles surface modification methods (Adapted from Ref 13)

The main reason for carrying out surface functionality of NPs is to develop biofunctional materials with new functionalities. A major functionality of polymers attached to surface modified inorganic nanoparticles is the intercalation of the lipophilic part with the existing aliphatic chains, covering or almost completely encapsulating

them.[4,5] Treatments using ozone, plasma or UV irradiation can also be used to add specific chemical groups onto the surface of NPs for later conjugation to biomaterials. Another technique involves the coating of nanoparticles with polyethylene glycol (PEG) to improve their circulation in the blood stream for tissue engineering applications. One study investigated the possible synergy resulting from the interaction between polymers and nanoparticle via the study of the generation of heat upon irradiation using thermal sensitive polymers and nanoparticles.[6]

Though the initial approaches have consisted of non-covalent adsorption of the macromolecules to the surface of the NPs, the method of using covalent linkages to the surface of NPs is favored.[7] Boissiere et al.[8] successfully coated alginate/silica nanocomposite particles with PEG by covalently grafting PEG-bearing organosilane onto their surfaces. The method prevents protein adsorption, and enables prolonged circulation times improving its biocompatibility. Physical adsorption, entrapment, crosslinking and covalent attachment are among the techniques used to functionalize nanoparticles with enzymes, antibodies and other biomolecules. Bioconjugation plays a crucial role in therapeutics. Polymer-NPs bioconjugated as drug delivery vehicles, optimize the effects of the drug while reducing many undesirable side effects.[6] For biosensing applications, bioconjugation is of great importance, because it induces changes in electrical, optical and photonic properties of the material, making it very sensitive to biological events.[9] The plethora of materials available, biomolecules, polymers and nanoparticles along with the increase in novel and innovative techniques provides the tailoring of refined nanocomposites for specific bioapplications (Figure 1.3).

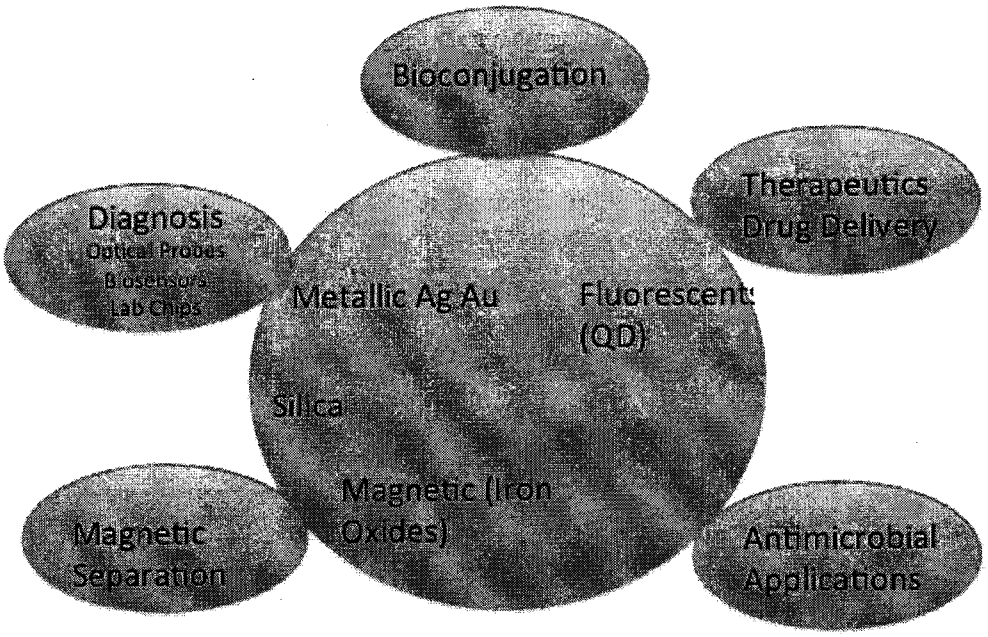

Figure 1.3 Examples of biomedical applications of nanocomposite particles (Adapted from reference 13).

There are several polymerization techniques that are used to prepare particle-based nanocomposites. One can take advantage of the hydrophobic colloidal stability of organically passivated NPs to prepare nanocomposites using miniemulsion polymerization.[10] nanocomposites are made by co-solution blending of the polymeric material and NPs using miscible solvents. The introductions of specific bio-chemical groups such as carboxyl, thiol or hydroxyl ligands are used for further attachment of bioactive compounds. Martins et al. investigated the use of miniemulsion polymerization to encapsulate a ferromagnetic nanocomposite, comprised of $CoPt_3$ nanoparticles and poly(tert-butylacrylate).[11] Later, the NPs were hydrolyzed using the ester group present

on their surface for further conjugation of antibodies via the renowned carboiimide-mediated reaction.[8]

Block Copolymers. In order to fabricate high performance devices, it is crucial to achieve an effective control over the self-assembly of copolymers. The flexibility in the molecular backbone of copolymers exhibits a Gaussian coil shape furthering their use in nanolithography, nanopatterning and templating along with the development of tailored thermoplastic materials.[12-14] To broaden the types of functional structures that can be obtained, the incorporation of inflexible rodlike shaped polymers was added.[13] Incorporating rod-like or coil shape functional polymers into block copolymers yields rod-coil block copolymers. Rod-coil block copolymers material introduce a wider variety of chemistries for an array of applications, i.e., photovoltaics and optoelectronics.

Block copolymers have the ability to self-assemble into intricate higher order structures. Self-assembly is a bottom up approach, where the molecular components undergo spontaneous spatial reorganization influenced by interactive forces. The properties and thermodynamic behavior of rod-coil polymers have been of strong interest for decades; however, these systems are very challenging to synthesize and results in low yields, hindering characterization techniques such as rheology that requires large sample loadings. In a review done by Bradley D. Olsen and Rachel A. Segalman[15] on the self-assembly of rod-coil copolymers, they explicate that because of the effect on chain topology on conformational entropy and molecular packaging geometries, rod-coil copolymer self-assembly is fundamentally different than that of coil-coil copolymers.

Inflexible chain structures, for example, semiconducting polymers and helical secondary structures (biomolecules) lead to the adoption of extended rigid chain conformations. The extended directionally dependent nature of rodlike chains extends the anisotropic interaction between the blocks enabling their ability for liquid crystalline ordering and crystalline phase separation. The liquid crystalline ordering of the rod blocks promotes a microphase separation between the mismatched geometries of the rod and coil polymers. The formation of micelles occurs in most block copolymer solutions as the solvent usually favors one block over the other resulting in rounded borders to decrease the interfacial contact between the solvent and the less soluble block. By comparison self-assembly of rod-coil copolymers in a coil favorable solution also form micelles; however, it results in liquid crystalline defects at the curved interphase. While much is known about polymer material preparation, not much is understood about how to tailor polymer structures to control self-assembly.

GONRs. While the use of graphite dates back to 6,000 years, an isolated single plane graphite dates back to the 1960's, when surprisingly higher basal-plane conductivity of graphite intercalation compounds were discovered.[16-18] Since graphene is a zero-gap material, their uses in semiconductor devices are limited. Graphene materials with energy gaps can be produced in two ways: controlled oxidation of graphene by a few layers or gold nanoribbons (GONRs). However, the production of GONR's with narrow width and smoothed edges are predicted to have band gaps allowing for further incorporation into transistors at room temperature. It must be noted that the Mullen's has made a significant breakthrough in synthesizing 2-dimensional GONRs 12 nm in

diameter using the Suzuki-Miyaura method (122). FET made from intrinsic semiconductor zigzag ribbons are predicted to exhibit a high level of performance with subthresholds as low as 60 meV per decade and transductance of 9.5 x 10^3 S/m.[19]

E-beam lithography is the most straightforward method to produce GONRs with a width of 20 nm from graphene sheet. Using single-walled nanotubes (SWNTs), a seamless approach of unzipping the tubes by an argon (Ar) plasma etching method was utilized by Dai et al. Using their approach, on a substrate, multi-walled carbon nanotubes (MWNTs) were embedded in a poly(methylmethacrylate) (PMMA) layer. A narrow strip of MWNT was left behind after the PMMA-MWNT film was peeled off using potassium hydroxide. The strips were later exposed to Ar plasma treatment where the exposed MWNT area was etched faster than the embedded nanotubes leading to unzipped GONRs. The PMMA film and residue were removed leaving behind single and multilayer GONRs with inner SWNT cores. Once the GONRs were fabricated into FET devices they exhibited quantum-confined semiconducting properties with much weaker gate modulation of conductance. The ratio of D band to G band (I_D/I_G) has been found to range from 0.28-0.38.[19]

Through oxidation and longitudinal unzipping of MWNTs in sulphuric acid, followed by treatment in $KMnO_4$ the production of GONRs was conducted by Shimizu and coworkers.[20] The oxygen groups were removed from the bulk and edges of the nanoribbons using a three-step annealing process. The first step was carried out to remove most of the oxygenation from the GONRs at 800 degrees Celsius followed by,

further annealing at 750 degrees Celsius in a hydrogen rich environment to terminate the edges and charge carrier doping before the fabrication of FET electrodes. The third step consisted of annealing the GONRs at 300°C to clean the surfaces before producing the electrodes. AFM images show a thickness of 0.8 nm and small structural defects caused by uncompleted removal of the oxidized groups as observed by HRTEM studies. The I_D/I_G has been shown to be ~ 0.45 suggesting a high quality of GONRs. The pioneering of GONR with controlled structure and tunable properties have been obtained various novel unzipping methods.

Thermal properties of Composites. The associated gains in thermal stability are critical for many applications as the change in the glass transition temperature provides insights into the fundamental changes in polymer dynamics. Various groups have investigated the change in thermal properties with the addition of nanofillers. The Rensselaer group examined the effect of coated and uncoated Al_2O_3on the glass transition temperature of PMMA. [21, 22] They found that at concentrations greater than 0.5 wt.% there is a significant drop in T_g of about 25°C when using uncoated Al_2O_3.

The Brinson group synthesized functionalized graphene sheets (FGS) and expanded graphite (EG) PMMA composite to study their thermal properties at very low loadings (~ 0.05 wt. %).[23] Functionalized graphene sheets were prepared by rapid thermal expansion of completely oxidized graphite oxide. FGS has a high-surface area of 600-800 m^2g^{-1} in the dry state and significantly higher surface area of 1,850 m^2g^{-1} in ethanol.[24,25] As oxygen functionalities improve the overall interaction with polar

matrices, single sheets of FGS have been found to be partially oxygenated, retaining a wrinkled topology. The second filler was produced by subsequent heating of sulphuric acid-intercalated graphene yielding expanded graphite (EG). These nanofillers are nanometers thick rigid nanoplatelets composed of graphene sheets held together by van der Waals forces. Well-dispersed graphene-based particles should result in viable nanocomposites with excellent thermal and mechanical properties.

The comparative study revealed very different thermal behaviors for nanocomposites made with FGS and EG. FGS composites exhibited an unprecedented shift of about 30°C at a 0.05 wt. % loading. The paramount increase in the T_g is linked to surface distortions of the FGS sheets after functionalization. These surface defects would likely result in mechanical interlocking with the polymer chains leading to better adhesion.[23] Further, FGS has hydroxyl groups that cover its surface providing further interaction with PMMA via the polymer's carbonyl group. In contrast, there was a decrease in the glass transition temperature for the composites made with expanded graphite. The depression in temperature is attributed to the thickening of the platelets and consequently decreasing the amount of surface area that is in contact with the PMMA matrix.

1.3 Self-assembly of Nanostructures

Although the design and fabrication of nanocomposites with flexible and controlled properties are an ongoing challenge, the incorporation of functional nanoparticles (NPs) into polymers is one of the most important means for enhancing

material properties.[26-29] The properties of nano-meter sized inorganic crystals or NPs are dramatically different from the conventional molecular and bulk materials due to the quantum confinement effect.[30,31] One can easily control NP functionalities simply by tailoring the dimension, thus their properties are inherently dependent on size. Nanoparticles have potential use in many areas: optical and electronic devices such as quantum computers, light emitting diodes and solar cells. Preformed NPs are usually in colloidal solutions or solid powders with a tendency to aggregate hence their potential use in applications are very limited.

Implanting NPs into inert media such as polymers decreases their surface activity making them less reactive and therefore, stable. A polymer intrinsic worth includes its physical and chemical stability, optical transparency and most of all it's compatibility, thus they are excellent candidates for the preservation of NPs functionalities. Furthermore, polymers are a great host material for different NPs with different functionalities.[32] Due to an array of particle size, it is possible to fabricate composites of various scales ranging from macroscopic bulk to microscopic patterns, and even to nanometer structures. [33-35] While NPs are inorganic materials, they can enhance the performance of organic polymer materials, although their properties are quite different. Inorganic materials will be able to subsidize the thermal stability of polymers through their high melting points, mechanical strength and refractive index. Nanocomposites enhance functionalities such as high refractive index strong photoluminescence (PL) and optical nonlinearity have been fabricated on the basis of molecular design, polymer preparation, and incorporation method.[36-40]

A plethora of methods have been developed for incorporating functional NPs with polymers,[41-43] such as directly blending NPs with polymers[44,45] *in situ* formation of NPs within polymer media,[36,46] copolymerization of surface modified NPs with monmers,[37,38] grafting of polymers onto NPs surfaces[47-50] and self-assembly of NPs and polymers through various weak supramolecular interactions.[51-54] In the *ex situ* process nanoparticles are made by an external step, added to the monomer or resin then later polymerized as shown in Figure 1.4. In this case, the nanoparticles are used as produced or delivered which tend to pose the most difficulties regarding agglomeration. Therefore, an additional step is necessary to surface functionalize the nanoparticles to optimize dispersion and interface chemistry; fundamentally enhancing the thermal and mechanical properties of the materials' matrix. Ford et al. prepared SWNT- polystyrene composites by lightly oxidization of the nanotubes via sonification in nitric acid. The SWNT were later dispersed in DMF and added to the polymer to prepare the composites. The samples were precipitated in 10-fold excess H_2O, filtered using PTFE membrane and dried at 110°C for one hour[55]. Mahdavian et al.[56] encapsulated commercial Al_2O_3 nanoparticles using an emulsifier with styrene/MMA followed by sonification and later, miniemulsion polymerization. Other approaches apply coupling agents to commercial nanoparticles and subsequently blend the particles with polymer powder leading to "bulk" composite materials.[57]

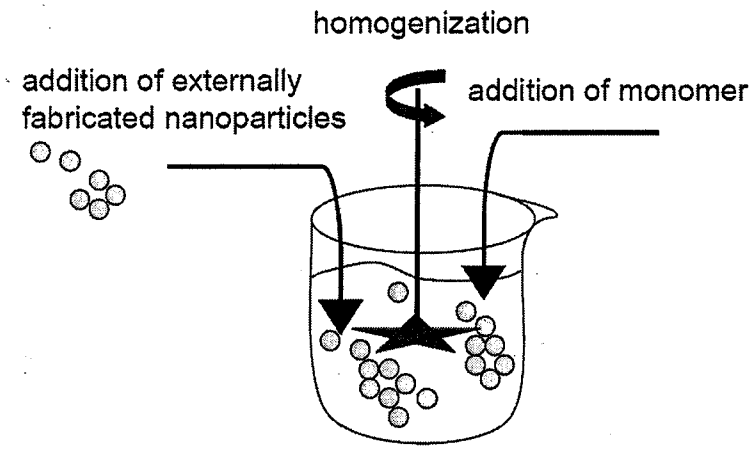

Figure 1.4. Sketch of dispersing nanoparticles in a monomer, polymer or resin by use of external shear force i.e. stirrer or by sonification prior to polymerization (reprinted from reference 58).

Another alternative to nanocomposite formation is the *in situ* approach. This method uses chemical reactions in a liquid environment to generate nanocomposite particles or compact nanocomposite materials. In the early 1990's through the use of synthetic ion exchange resins and an aqueous solution of Fe (III)-chloride, a one-step chemical method to synthesized fine dispersed Fe_2O_3 nanoparticles in a cross-linked polystyrene resin was conducted by Ziolo et al.[59] Gonsalves et al.[60] in contrast, synthesized AIN nanoparticles using a sol-gel method then later applied an effective solution mixing method to generate a homogeneous dispersion of AIN nanoparticles in polyimide. The difference between the two methods mentioned above is the functionalized nanoparticle in the latter procedure is synthesized in the first step in a solution followed by the addition of the monomer and brought to polymerization.

The easiest method to obtain omnifarious structures in comparison to other method is through self-assembly.[61-66] Self-assembly fabricated various nanocomposites such as layer by layer (LbL) deposition ultra thinfilms,[67,68] microspheres,[69,70] capsules,[71] vesicles[72] and micelles. [73-75] These supramolecular forces are made up of weak intermolecular interaction such as H-bonding, dipole and van der Waals interactions.[34,35] There is a possibility to further moderate the process of self-assembly by controlling assembly and disassembly because these weak interactions are sensitive to any variations in their environment. Through the combination of microfabrication techniques for example soft lithography, microcontact printing, template-induced assembly, and other derivative methods, nanocomposites can be fabricated in different size, shape and even to complex structures.[76-80]

Formation of nanocomposites via van der Waals interaction. NPs functionalities are synthesized with desired amenities namely, size, shape, surface chemistry and through a bottom-up assembly method to prepare nanocomposites. NPs prepared through a synthetic route using the organometallic route are capped by fatty acids producing lipophilic alkyl chains on their surfaces allowing their compatibility with lipophilic polymers via Van der Waals interactions. Direct blending of nanoparticles and functional polymers were driven by the requirement of organic-inorganic hybrid light-emitting diodes (LED) and is an example of the bottom-up fabrication of polymeric nanocomposites. Because of the hydrophobic interaction between the alkane of NP ligand and the alkane of the polymer, both constituents exhibited efficient compatibility

allowing an efficient transfer of electrons along the NP/polymer interface leading to the eventual development of composite film with photoelectric or photovoltaic properties.[81,82]

Combing the self-assembly behavior of amphiphilic copolymers and the hydrophobic nature of NPs, composite vesicles and micelles can be fabricated.[83,84] Block copolymer possesses both hydrophobic and hydrophilic blocks therefore, the hydrophobic block will interact well with the hydrophobicity nature of NPs. When exposed to polar solvents the hydrophobic blocks assemble with the alkanes attached to NPs through hydrophobic-hydrophobic interactions, while the hydrophilic blocks spread around the surroundings to make the composite structure dispersible in water.[85] Forming such composite micelles lead to the construction of hydrophobic metals, metallic oxides, and semiconductor NPs. Gao et al. established a novel method to fabricate multiplexed nanobarcodes through crosslinking of individual composite micelles that contained maleic anhydride groups where the micelles grew epitaxially into nanobeads with narrow size distribution.[86] Constructing various nanostructures will give new opportunities in NP-based ultrasensitive detection and imaging using the innovative step-wise self-assembly technology.

The driving force for self-assembly of surfaced-charged NPs with oppositely charged polymers are achieved via electrostatic interactions. Layer by layer (LbL) assembly, an efficient method to obtain ultrathin films with thickness in the nanometer range is the first example of self-assembly compelled by electrostatic interaction.[43,87] Layer by layer assembly can be fabricated on many substrates including glass, silicon,

quartz where the film thickness increase is only in the nanometer range by controlling circular times. MPA-coated luminescent CdTe NPs have been assembled with positively charged poly (diallyldimethylammonium chloride) (PDDA).[88,89] CdTe NPs can be tuned to different colors from green to red enabling the fabrication of distinct PL or electroluminescence. Because all the building blocks of LbL assembly contain charges it is possible to moderate assembly through the promotion or suppression of electric fields. Though electrostatic interactions are weak, the LbL assembly can be altered to covalent linkages by further thermal crosslinking or photoreaction greatly enhancing the permanence of practical applications.

Self-assembly of Polymeric Microcapsules. Self-assembly of polymeric microcapsule either by the formation of polymersomes or colloidal emulsion templating lacks stability, monodispersity and high loading efficiency limiting both their function and subsequent applications. Through one step supramolecular host-guest chemistry (Figure 1.5), microcapsules using Cucurbit-uril (CB) exhibited stimuli triggered degradation, higher loading capacity and monodispersed droplets proving potential use in diverse applications such as drug delivery, cell encapsulations, diagnostics, etc.[90-93] CB is a host molecule capable of forming stable yet dynamic complexes with high affinity guest compounds in water.[94,95] Zhang et al reported the preparation of microdroplets using CB and two guest molecules in a 1:1:1 teranary complexation in water achieved through multiple non-covalent interactions.

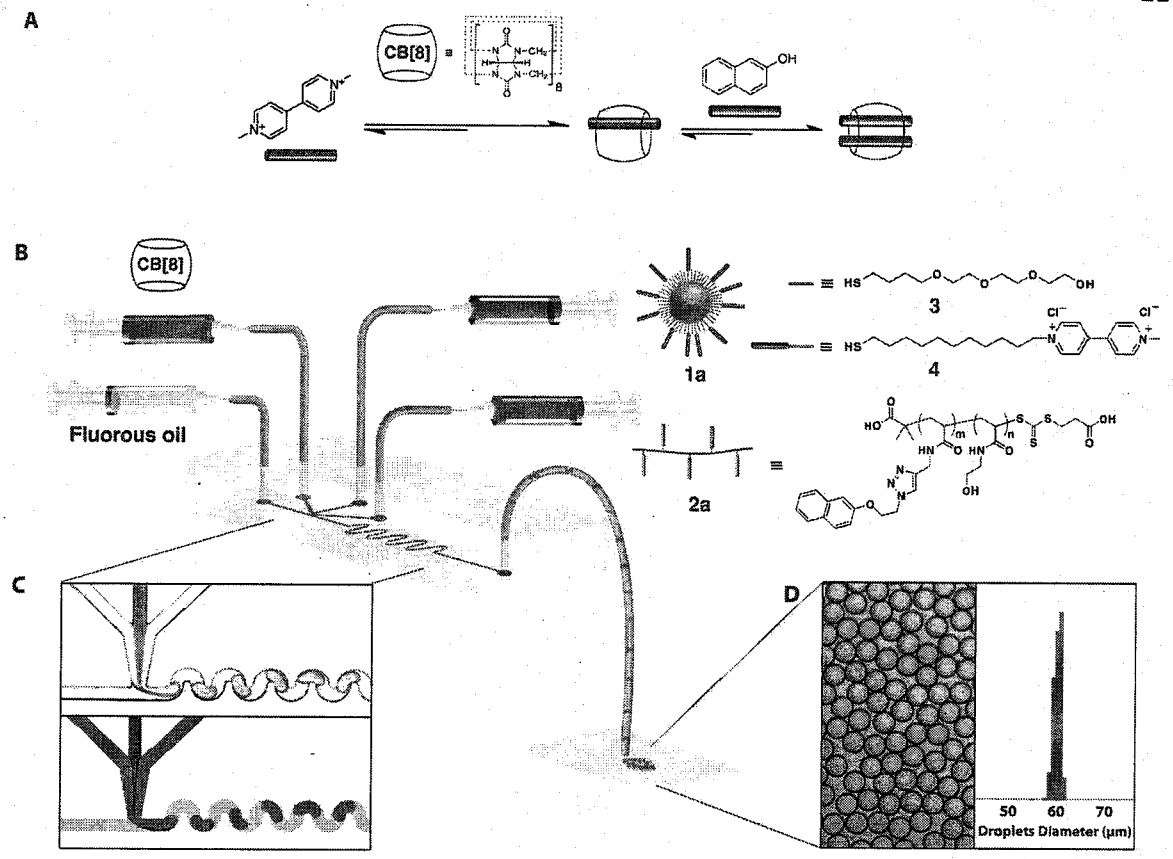

Figure 1.5. (A) The two-step, three-component formation of the CB [8] ternary complex in water with MV2+ (blue) and Np (red). (B) Schematic representation of the microdroplet generation process using a microfluidic T-junction device, consisting of an continuous oil phase perpendicular to a combination ofthree aqueous solutions of CB[8], 1a (AuNP functionalized with a mixture of neutral and viologen-containing ligands 3 and 4), and 2a (copolymer functionalized with Np) as the dispersed phase. (C) Microscopic image and the schematic of the T-junction and a wiggled channel for rapid mixing of reagents online. (D) The high monodispersity of microfluidic droplets is demonstrated by the narrow size distribution (diameter 59.6 T 0.8 mm) (reprinted from ref 106).

The first guest Methyl Viologen (MV2+) along with derivatives of napthol an electron-rich molecule and CB comprised the microcapsules or complexes.[96] To further exploit CB's functionalities, it was used as a supramolecular handcuff to hold and control dispersion of gold nanoparticles (AuNPs) within a water-soluble copolymeric network[97]

A simple T-Junction shape microfluidic device produced microdroplets using two phases: oil and aqueous. The oil phase was perpendicular to the aqueous phase, which had three inlets for the CB, MV AuNPs and the polymer nanocomposite. Monodispersed droplets were achieved by the shearing of the oil phase off the aqueous phase while simultaneously controlling the flow rate of the oil and aqueous phase using a ratio of 2:1.

After two minutes the droplets collected onto a glass slide collapsed as the spherical shape of the droplet became slightly distorted due to evaporation of the aqueous phase. Via Scanning Electron Microscopy (SEM) it was shown that a dry hollow capsule was left behind due to the lack of internal support. The capsule shell was then investigated confirming a supramolecular self-assembly network of AuNPs and copolymer where individual AuNPs were interlinked via a mesh formed by the polymer as a result of interfacial tension stabilization.

1.4 Supramolecular Constructs

Research into the design of supramolecular assemblies to assist in treatment of diseases with poor prognosis such as cancer, cystic fibrosis and viral infections has increased in recent years. Although a number of novel potent natural, synthetic or semisynthetic low molecular weight drugs have been developed, converting those to therapeutic agents has been challenging. Poor biopharmecuetical properties, low absorption through bio-membranes, and a need for rapid elimination from the body have prevented the transformation of biotech drugs into medicines.

Modern polymer-based nanotechnology offers potential opportunities in the treatment of diseases through the use of new molecular scale medical interventions that can be applied to produce tailor-made nanomedicines for improved therapies and personalized treatments.[98-101] Polymers are multivalent allowing for customization with drugs, targeting agents, and cell penetration enhancers amongst others. These heterogeneous constructs offers a variety of physiochemical and biological properties that can be exploited to produce novel colloidal therapeutic systems.[102] One advantage of the use of polymeric materials as therapeutic proxies are their high molecular weight which allows prolong absorption through bio-membranes, and accumulation at infected sites such as tumors or inflamed tissues. Some examples of polymer-based nanomedicines are polymer-protein bioconjugates, polymer-DNA complexes and polymer-drug conjugates. It is imperative to note, that polymers are used to create new drug carrier platforms such as micelles and nanoparticles with specific or smart biopharmaceutical features.[103]

New interests and perspectives in the treatment of a vast array of diseases have been revolutionized through the use of proteins as therapeutic agents. Comprehension of their structure and functional mechanistic relationship, an increasing number of protein drugs and biosimilars have been elevating the pharmaceutical arsenal. Low physiochemical, immunological and biopharmaceutical properties of protein macromolecules limit their exploitation in medicine.[104,105] Physical, chemical or enzymatic inactivation usually occurs during fabrication, manipulation, storage and delivery of proteins due to their delicate structure. Their hydrophilic properties and large size significantly limit their permeation through biological membranes usually resulting

in their rapid elimination from the bloodstream. Excretion of these macromolecules from the body occurs in various ways; glomerular ultrafiltration, liver up-take, and degradation. Lastly, their intrinsic immunogenic and antigenic characteristics forces them to be removed from the body as well as inactivated or converted to toxic products by the immunosystem.[105,106] Presently, several techniques have been explored to fix or alleviate the biopharmaceutical profile of proteins as well as provide for suitable delivery, such as micro and nanoparticle encapsulation and polymer conjugation.[105,107] When compared to the parent molecule, enhance therapeutics performance has been achieved through protein-polymer conjugation.

Particular efforts have been made over the years to set up efficient and selective conjugation methods resulting in derivatives that will exhibit suitable physicochemical and biopharmaceutical properties that meet the standards of regulatory agencies globally. 5kDa of PEG was randomly conjugated with short polymer chains to the surface of proteins. To produce conjugates with biopharmaceutical and immunological properties extensive conjugation was required with low molecular weight of the polymer. Since amino groups are exposed on the surface of proteins, PEGylation was achieved through multiple polymer attachment at the reactive site.

Superoxide dismutase (SOD) an enzyme has interests in therapeutic applications for the treatment in diseases such as inflammation that exhibits over production of superoxide ions. Rapid elimination of SOD and high immunogenicity has severely limited their use, however; with extensive protein PEGylation those problems are overcome. In an animal study using rats PEGylaton of SOD have been found to prolong

blood circulation resulting in 25 hours blood half-life compared to that of the parent molecule. Increased protein bioavailability along with a decrease in antigenic character and immunogenicity occurred as result of polymer conjugation. The high number of polymer chains conjugated onto the protein surface, showed only a small decrease in enzymatic activity and the bioconjugate was found to be effective in different therapeutic pre-clinical trials.[108] The production of first generation PEGylated products was introduced to the market in the 1990s by Oncaspar and Adagen corporations.

Using Avidin as a protein model, the physicochemical, biopharmaceutical, and immunological properties were studied as a function on the effect of polymer size and shape. Avidin was conjugated using 5 kDa linear, and 10 kDa branched polymer chain attached to 10% of the available amino group to reduce the immunogenicity and prolong its stability in the bloodstream. The findings revealed, PEGylation reduces the renal clearance and the liver up-take while promoting bioconjugate accumulation in solid tumors by enhance permeation and retention (EPR) effect.[109] The mass of the polymer associated with the protein strictly related to the pharmacokinetic, immunological and biological properties. As the PEG molecular weight increases, so does the prolong permanence in the circulation (Figure 1.6). The PEGylated forms of Avidin obtained from 10kDa and 20kDa are a promising product for therapeutic applications.

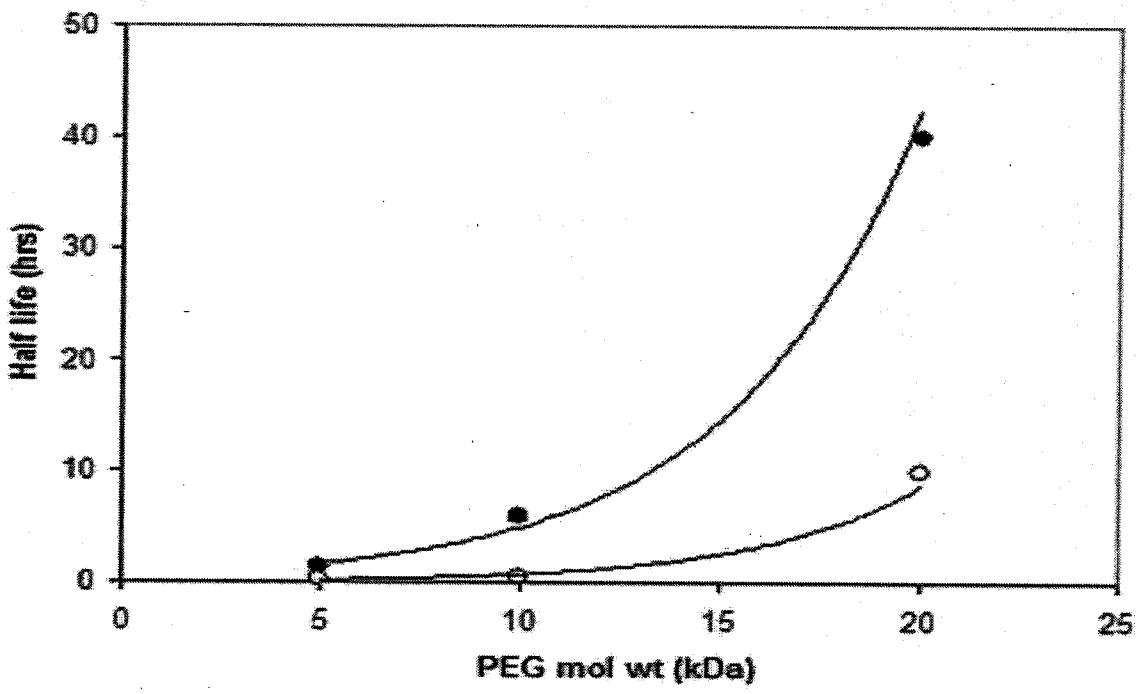

Figure 1.6 Plasmatic half-life of 5-, 10-, and 20-kDa PEG modified avidin after intravenous injection to mice. Avidin modified with 4 PEG chains (*), avidin modified with about 16 PEG chains (Reprinted from ref.146).

Irrespective of multiple PEGylated chain conjugation or by using high-molecular-weight polymers, as the polymer weight increases the immunogenicity decreases and the lastingness time in the circulation increases.[110] The balance between polymer and protein mass is mainly relevant in order to produce derivatives with enhance biopharmaceutical and immunological properties that exhibit high activity since it has been found that with the increase in polymer mass there's a consequential decrease in biological activity.[107,111] In the case of cytokines and antibodies that operate with high-molecular weight receptors polymer to protein mass must be taken into deep consideration. A suggestion to the findings mentioned above is the use of protocols that entail site-selective polymer attachment or active site protection. Urokinase and trypsin were used as protein models

for heterogeneous phase site protection.[112,113] Protein PEGylation was carried out in the presence of a Sephadex™ resin functionalized with the enzyme inhibitor benzamidine, which allowed for protein reversible attachment to the resin and simultaneously protected the active site from polymer modification.[114] The polymer conjugation method resulted in a high degree of reactivity with the extensively modified proteins produced.

Through the use of large soluble and insoluble inhibitors, active site protection is achieved preventing polymer attachment in the area of the protein binding sites. Figure 1.7 shows the structure of biotinylated-PEG that was synthesized to protect the avidin recongnition site during polymer attachment. The bioconjugates displayed increase permanence in the bloodstream after intravenous injection and complete suppression of the avidin immunogenicity and antigenicity.[114] Using 10 and 20 kDa PEG, there was a 70-80% of the proteins ability to interact with biotinylated antibodies via the use of active site protectors; whereas using 5kDa PEG there was only a 20-40% of the native biorecognition properties retained in products obtained without active site protection. Without the active site protectors, PEGylation of Lys amino groups were found near the vicinity of the biotin recognition region which may have accounted for the insubstantial biorecognition properties. However, even in the presence of a protecting group, the low activity of derivatives obtained with 5kDa PEG was probably due to the small size of the polymer which can approach the binding site and react with Lys irrespective of the existence of the protecting agent.

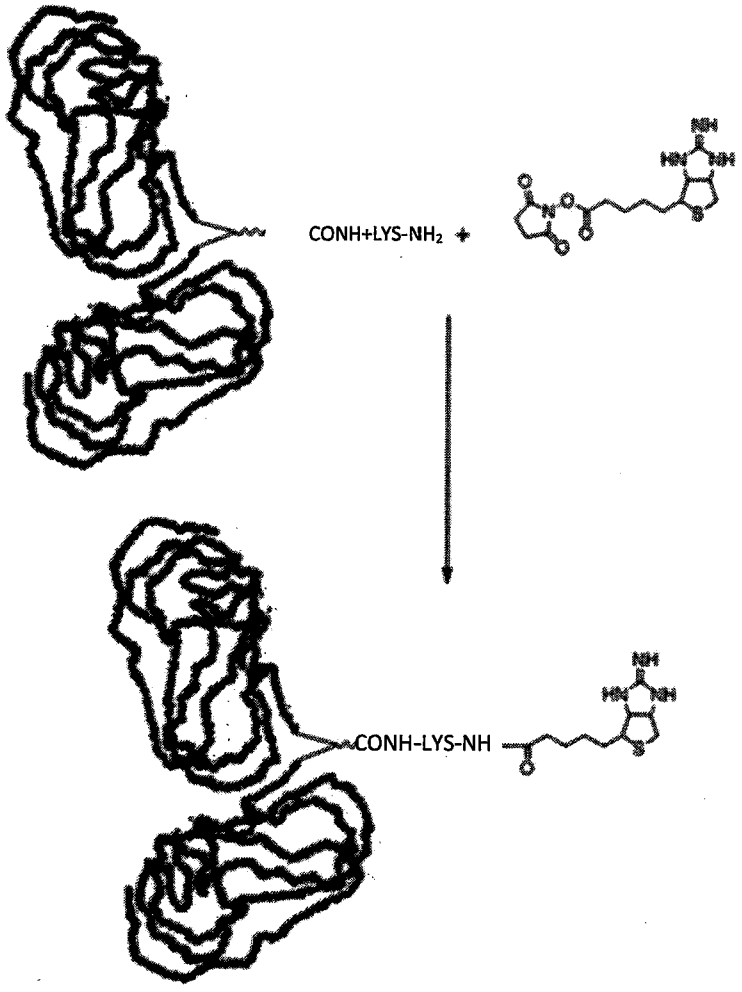

Figure 1.7 Synthesis of biotnylated branchched 20 kDa PEG (Reprinted from ref. 112).

Tailor-made PEGylated derivatives with well-defined structure and composition with high biological activity have been proposed using several techniques. Through polymer anchoring to rare amino acids along the protein sequence site, selective PEGylation is accomplished. Neulasta® the rh-GCSF-PEG derivative available on the market was an example of site-selective modified protein prepared under reductive conditions with end-terminal aldehyde functionalized linear 20-kDa PEG.[115] The

exploitation of the lower pKa of the amino group compared to that of lysein promoted terminal amino group conjugation.

Cysteine (Cys) residues are less likely to be represented in protein structure, however; they have the propensity to be artificially introduce into proteins by site-directed mutagenesis of the primary sequence, for this reason, cysteine conjugations is one of the most interesting and versatile technique for selective protein PEGylation. Various PEGylated proteins such as antibody fragments and engineered proteins have been developed through the exploitation of Cys to polymer anchoring using numerous approaches for thiol conjugation.[116,117] Cys amino acid is located deep within hydrophobic pockets sterically hindering protein dimerization through disulphide binding. Large molecules like PEG are difficult to conjugate because of Cysteine's unreachability, nonetheless; a novel end-hydrophobized PEG has been synthesized and investigated using rh-G-CSF to eradicate this setback.[27] Based on the structural properties of the hydrophobic pocket hosting the free Cys of rh-G-CSF, the hydrophobic arm linker was chosen to facilitate the PEG docking to the amino acid. When comparing the end-hydrophobized PEG to the commercially available maleimide-activated polymer, the former shows successful conjugation to the Cys group of about 60%, while the latter only yielded about 20% protein conjugation. The end-hydrophobized PEG along with an increase in temperature resulted in faster conjugation as the polymer can form micellar assemblies that forces the maleimide group into the hydrophobic core confining the polymer reactivity to the thiol groups. The end-hydrophobized polymer is stable under stressing shear force conditions supporting the claim that the penetration of the

hydrophobic spacer does not evoke intense structural alteration, a supreme requirement for protein stability and activity. Bioactivity studies showed that the end-hydrophobized polymer slightly decrease cytokine activity which may be attributed to the steric hindrance of the high molecular weight polymer, however; the results are comparable to the biological studies of Neulasta®.

Protein engineered procedures, tag based procedures or enzyme-mediated PEGylation are other approaches used for site-specific PEGylation.[118,119] Transglutaminase and carboxy peptidase have been exploited to PEGylate glutamines and terminal carboxylic moieties exposed on the protein's surface.[30, 31] PEGylation procedures have been recently divulged by Neose Technologies which involves selective glycosolation of serines and theronines in proteins expressed without glycosydic unit such as *Escherichia coli*, followed by sialic acid derivatized PEG to the introduced N-acetyl galactosamine (GaINAc) residues by sialyltransferase.[120] Maltosyl and lactosyl-based linkers have been synthesized and conjugated to hidden protein sites for multiple poymer attachment using a new protocol which involves the chemical insertion of glycosyl functions into protein structure followed by PEGylation of the oligosaccharide tag.[121] Figure 1.8 depicts the small glycosyl linker attached to the Cys was activated by selective oxidation with periodate, which switches vicinal diols into aldehyde groups followed by conjugation with PEG-Hz reacting with aldehyde moieties to form reversible hydrazone bonds.[122,123] The percent conversion to PEGylated proteins was over 90% for the glycalated species reaffirming that the mixture of site specific PEGylation may have

numerous rewards in the fabrication of therapeutic bioconjugates as it conglomerates the beneficial attributes of hyper-PEGylation with the nanomedicine model.

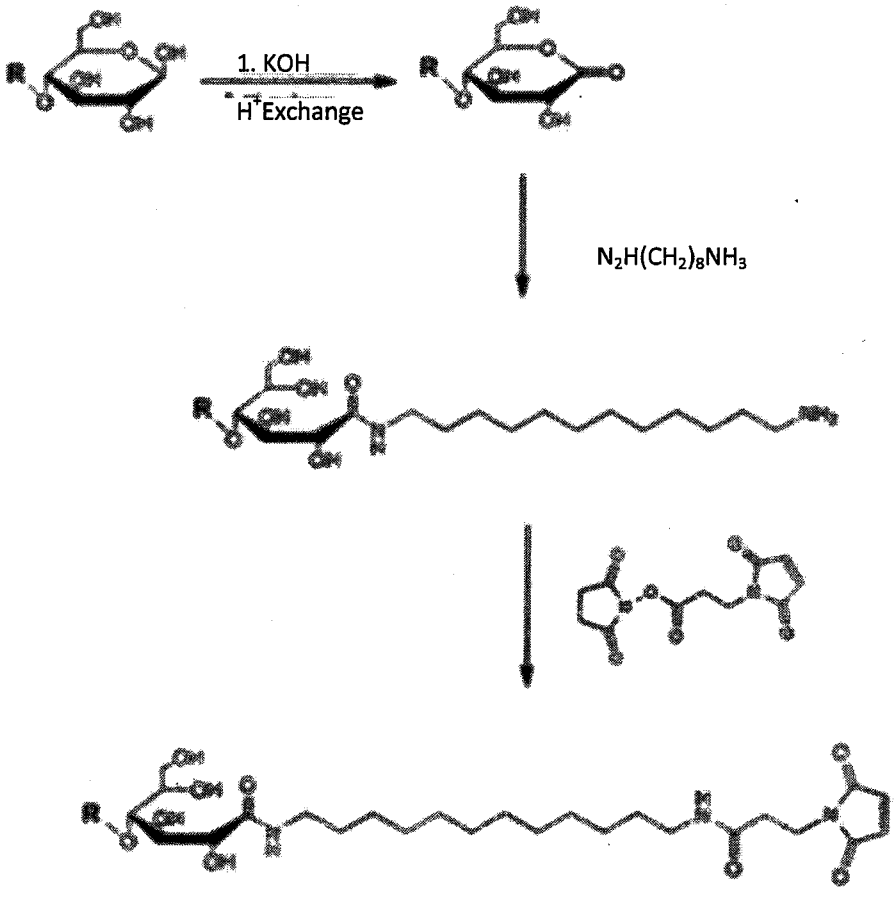

Figure 1.8. Synthesis of malimide activated glycosyl linkers (Reprinted from reference 119).

1.5 Nanostructures: Active Components in Sensors

Cardiovasular disease (CVD) is a group of medical ailments that involve the heart or blood vessels. Chest pains are the most notable symptoms of CVD. An electrocardiogram (ECG) is the first tests that most patients receive in the emergency

room to identify acute coronary syndromes (ACS). However, there are pit falls to using the ECG test, it lacks sensitivity and is unable to detect myocardial injuries. The uses of biomarkers to study myocardial infraction have been reported as early as 1954.[124] Presently, patients with potentially ACS problems are being tested with cardiac biomarkers. Assays such as enzyme-linked immunosorbent assay (ELISA) are used to detect biomarkers, but this technique has a very low throughput; taking a long time and suffers from large sample and reagent consumption. To subsidize these problems, the use of point-of-care (POC) devices which are rapid and relatively simple to use has emerged. The POC devices eliminates the need for ordering tests and sample transport to laboratories but, these test kits lack sensitivity pushing doctors to test multiple times for different biomarkers prolonging the much needed treatment to patients suffering from a heart attack. Additional strategies are required to detect ACS in a timely fashion in order to save heart attack patients.

Comparable to their sizes of biological species and chemicals, nanostructures such as nanowires (NWs), carbon nanotubes and nanoparticles have been widely used to investigate their potential as active components in biosensors. Commonly explored, nanoparticles have been used as an alternative to fluorescent labeling for the detection of bio-samples with great sensitivity. This process still suffers from target labeling as the addition of labels are time consuming and may cause steric hindrance. Nanowires and nanotubes offer the ability for real-time and label free sensing as well as their large scale sustainability and high density integrations.

Investigations into silicon nanowires (SiNWs) as a field-effect transistor (FET) sensor have raised a lot of interests over the last several years. This technology allows the detection of change in charges when analytes binds onto their antibodies immobilized on the surface of the probe. SiNWs large surface to volume ratio, biocompatibility and tunable electrical properties allows a highly sensitive, label free and specific detection. Upon antigen-antibody binding, the SiNWs senses the subsequent change in charge density inducing a change in electrical field. The process has been used to detect a wide spectrum of species ranging from metal ions,[125] proteins,[125,126] nucleic acids[127] and viruses.[128] The electrical-based biosensor combines biomolecules with complementary metal-oxide semiconductor (CMOS)-compatible a process that is highly sensitive and agreeable to mass production with low costs. The SiNWs sensors are fabricated much in the same way as a typical FET-base device containing source, drain and gate electrodes where the NWs are connected between the source and drain in the semiconductor channel. The semiconductor channel is configured differently in immunological-modified sensor with a uniform conductance based on the electron density in the n-type SiNW sensors as shown in Figure 1.9.

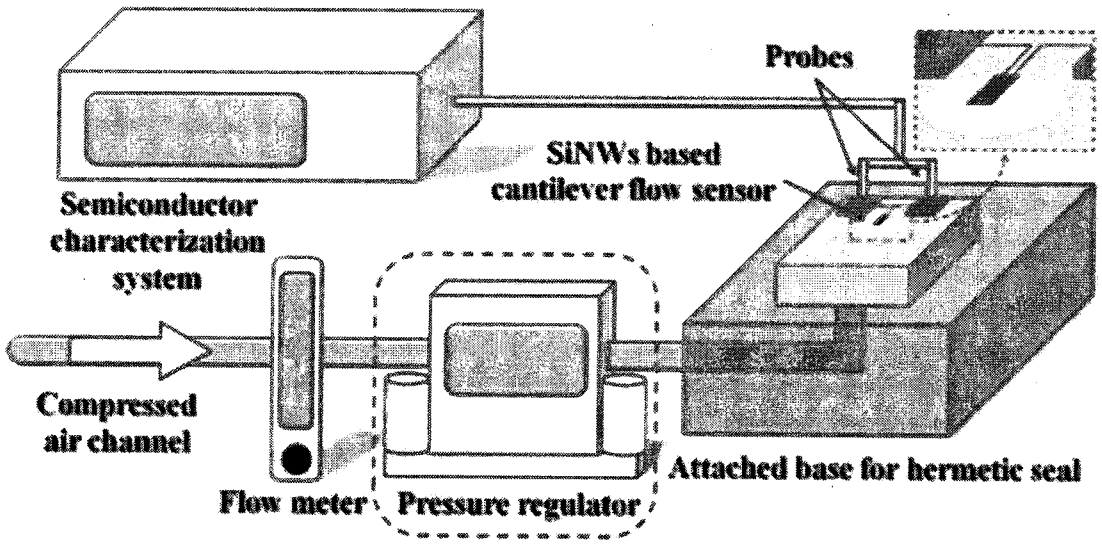

Figure 1.9. Principle of silicon nanowire (SiNW) biosensor. SiNW serving as the semiconductor channel is connected to the source and drain electrodes. Antibody Immobilized on the SiNW surface is capable of specifically recognizing and capturing the cardiac biomarker. When a negatively charged biomarker binds to the antibody, it repels the negative charges in the region of the nanowire, resulting in a decrease in conductance ref. from Zhang *et. al.*

There are two main fabrication technique employed to produce semiconducting NWs SiNWs biosensors. These fabrication techniques are top-down and bottom-up approaches. Stern et al found that NWs with small dimensions results in greater sensitivity indicating the need to produce fibers with diameters in the nanometer range for high performance sensors. The vapor-liquid-solid technique is a bottom-up approach used to forge n-type or p-type SiNWs in dimensions around 20 nanometers using gold nanoclusters as a catalysts and diborane or phosphine as a dopant precursor.[129] Though, the NWs grown on the silicon substrate were of high quality, they lacked uniformity with varying dimensions. E-beam lithograpy a top-down approach combined with the

superlattice NW pattern transfer (SNAP) method also yield the production of NWs. The NWs produced from the top-down approach are produced in high yields with a well-ordered orientation on the silicon substrate. The fibers average about 50 nm in diameter with lengths extending from 20 μm to 1mm allowing for great device uniformity. Through the use of CMOS-compatible technology, Zhang et al. fabricated individually addressable SiNWs in a perfectly aligned array format for better manufacturability and commercialization of SiNWs devices. The fibers are produced by photolithography using a wafer consisting of 72 individual SiNW sensor chip with 40 clusters of 5 nanowires each divided into two chambers as seen in Figure 1.10.

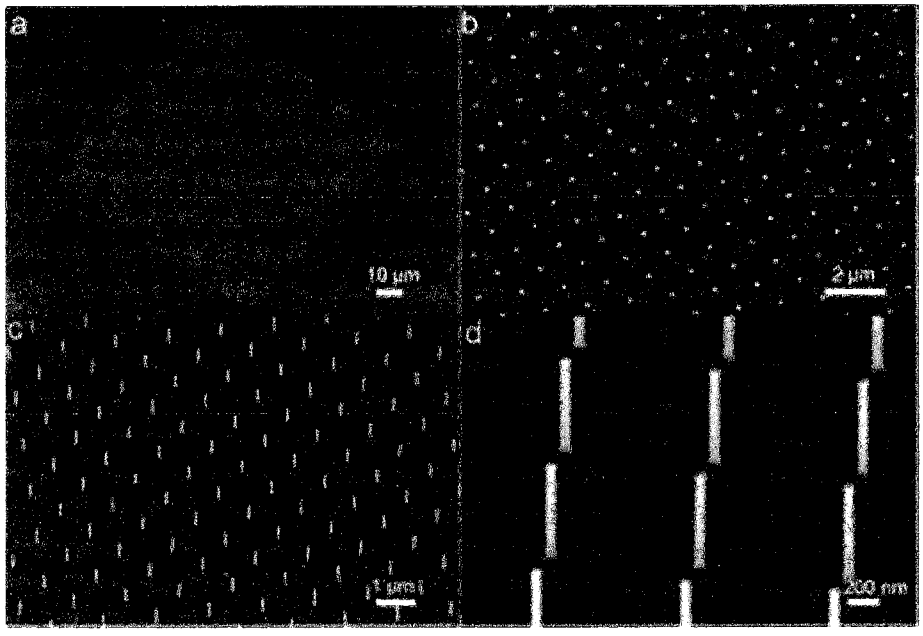

Figure 1.10. Silicon nanowire (SiNW) biosensor array chip. (a) Vertical silicon nanowire square array. Overall extent of nanowire array is 100 Ã‚,μm by 100 Ã‚,μm. Nanowire pitch is 1 Ã‚,μm. Top view (b) and 30 Ã‚,° tilted view (c) of nanowire array. (d) Magnified tilted view of nanowire array. The nanowires have radii of 45 nm and are 1 Ã‚,μm long. Credit: Courtesy of Ken Crozier and Kwanyong Seo, Harvard School of Engineering and Applied Sciences

Functionalization of the surface of the SiNWs for specific molecular recognition can be carried out in two ways electrostatic adsorption and covalent binding. Electrostatic adsorption is complete when an attractive force from the ionic solute is adsorbing on an oppositely charged adsorbent. DNA detection was achieved using SiNWs in an electrolyte solution in which primary DNA strand was electrostatically adsorbed onto an amine terminated organic monolayer atop the NW surface.[127] As the name suggests, covalent binding of the probe molecule is achieved via covalent bonds. Hydrogen-end terminated SiNWs are attained through submersion of the SiNWs in hydrofluoric acid. The end functional group can later transfer into a stable Si-C bond upon photochemical hydrosilation affording amino groups for later addition of proteins and DNA probes. 3-Aminopropyltriethoxysilane (APTES) a type of alkoxysilane is a well-known linker used to interact with the oxide layer on SiNWs upon functionalization. The reagent yields amino groups on the NWs' surfaces that can be used to immobilized PNA, DNA and antibodies for various sensing.[126,130] Antibody cTnT was functionalized unto the SiNWs' using APTES to bind the hydroxyl-terminated SiO2 surfaces of the NWs to produce an amino-functionalized surface. Glutaraldehyde a biofunctional linker was attached to the amino-functionalized surface for the addition of the antibody (Figure 1.11). The excess unreacted aldehyde groups were later passivated with ethanolamine to prevent non-specific binding of antibodies during the detection stage.

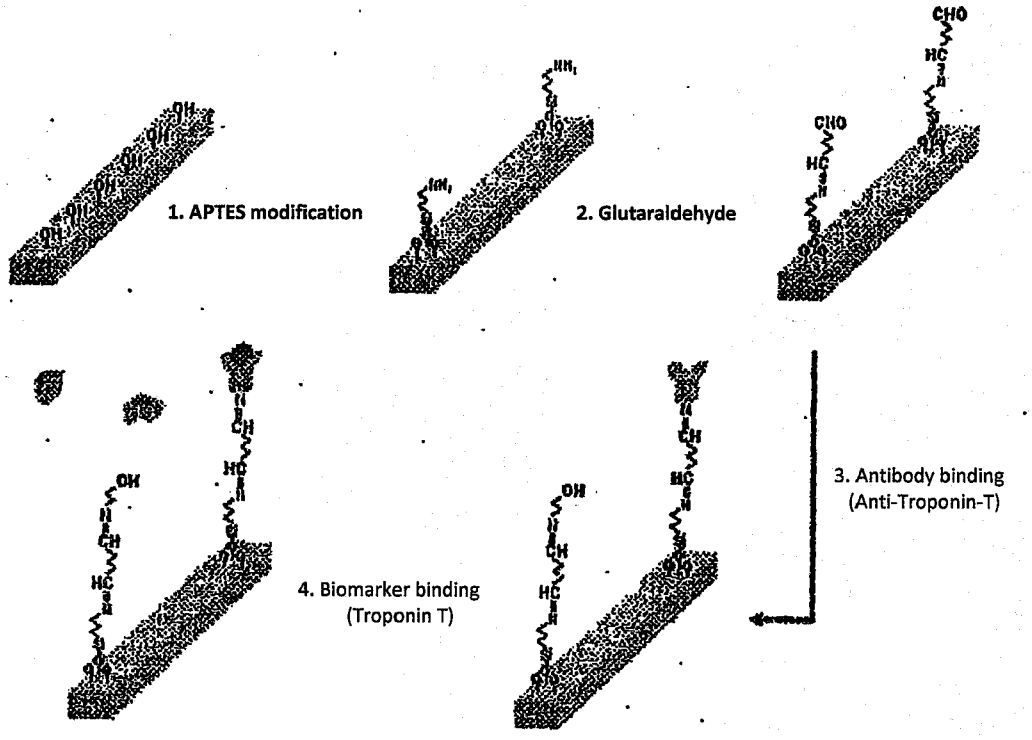

Figure 1.11. Schematic diagram of chemical process for surface functionalization of one silicon nanowire (SiNW) sensor. The hydroxyl terminated silicon dioxide surface of the nanowire binds to the ethoxy groups of 3-aminopropyltriethoxysilane. Glutaraldehyde converts the amino-terminated surface to an aldehyde-terminated one, which is able to bind with the N-terminus of the anti-troponin-T-antibody. Antigen-antibody interactions cause troponin T to bind specifically to the anti-troponin T probes on the surface, causing changes in SiNW conductance. (Reprinted from Chua et al. 2009 American Chemical Society.)

Delivery of the analyte to the sensor surface is accomplished through a fluid exchange system that comprise of two methods. An open chamber and a close microfluidic channel have been developed to direct the desirable analyte to the SiNWs. The most commonly used of the two methods is the latter. The close channel is usually made of polydimethylsiloxane (PDMS) where the solution is directed over the NWs

allowing a small volume of sample to be considered. Nonetheless, the microchannel system suffers inherently from the inability to deliver most of the analytes to the SiNW surface and prevent the target molecule from sticking to the PDMS channel walls. A rectangular micro-scale solution chamber made out of acrylic was used to overcome the challenges mentioned above. This system allows a larger amount of solution to be delivered from the top to the bottom of the NW sensor increasing the sensitivity of the construct. The cTnT antibody was delivered using a commonly used buffer solution for measurement phosphate buffer saline (PBS). With the pH of PBS being neutral, the cTnT antibodies negatively charged anions around pH 7.4 may cause the potential screening of the protein molecules by the counterions that exist within the buffer solution. For this reason, Debye screening is extremely pertinent to FET sensors because the Debye length can affect the device performance. The Debye length is the distance in which sufficient charge separation can take place. The length is expected to be long using a dilute buffer with salt concentrations so that less charge is screened. However, excessive dilutions with low electrolyte concentration may inactivate the biological activity of proteins. The Debye length is estimated using the following formula:

$$\lambda d=0.32(I)-0.5 \qquad (1)$$

Where I is the ionic strength of the buffer solution used for sensing. In conjunction with an HP parameter analyzer and a two-probe system voltage real- time detection was performed. A controlled voltage was applied to the source electrode of the SiNWs device with the drain electrode reference to the ground using the two-probe system. After the

buffer solution was injected through the inflow tube a short voltage of 0.1 was applied to the sensor and the current was measured. The current was monitored for 200 seconds to establish a baseline current for which changes in conductance will be measured. The biomolecule analyte was then introduced to the sensor via the inflow tube resulting in a change of conductivity due to specific antibody-antigen binding on the NWs surface.

Detection between various concentrations of cTnT were prepare by serial dilution in 0.01xPBS in order to develop a SiNW chip capable of detecting ultralow concentrations. Zhang et al. used blank buffer without the presence of cTnT and compared it to the sensor response of the lowest cTnT concentration of 1 fg/mL to evaluate the signal to noise ratio.[130] The lowest detection limit was therefore defined as 1 fg/mL for cTnT because it exceeded the background noise by three times.

Biosensors for medical point of care applications must be able to accurately detect low concentrations of biomarkers in human blood serum. Raw human blood serum was obtained from a healthy individual that had no prior history of heart disease and used for further testing. After desalting using Zheng et. al techniques various quantities of cTnT were spiked into aliquots to obtain the required analyte solutions.[131] A baseline was established using the desalt solution without cTnT to measure the conductance upon introduction of cTnT solution. The conductance of the sensor immediately decreased and subsequently stabilized at a lower value for 300 fg/ml to 30 fg/ml cTnT concentrations. Zhang et al. therefore, demonstrated a label free and real time detection of cardiac troponin T antibody in an undiluted serum environment down to the 30 fg/ml range three

orders of magnitude lower than ELISA detection methods which takes more critical time to determine.

Biosensor Arrays for Biodiagnostics. To generate a complex molecular profile for the diagnosis, monitoring, and prognostic evaluation of complex diseases such as cancer there is need for quantitation and identification of numerous biological molecules. Detection in the change of mechanical and electrical properties due to antigen-antibody binding is a technique for multiplex analysis of extracted proteins for disease monitoring.[131] Although this technique is capable of detecting protein interactions, it cannot be adopted to detect cancer among populations that are not close to a laboratory or a hospital without significant modifications and a highly trained personnel.[132] To design a portable handheld device for the diagnosis and treatment of cancer, one must employ an interdisciplinary approach; combining the knowledge of cancer biology, molecular targeting and nanotechnology.

Blood samples are taken of circulating cancer at advance clinical stages where Insulin-growth factor 1 receptor (IGF1R), and human epithelial growth factor receptor 2 (Her2) are over expressed in breast cancer growth and development.[133-137] Both Human BT474 and MCF7 breast cancer cells express IGF1R proteins and Her2 mRNA however, at different levels. High levels of Her2 mRNA are expressed on. Human BT474 breast cancer cells while IGF1R proteins are overly expressed on MCF7 breast cancer cells. The author reports that this is the first time where the detection of BT474 and MCF7 breast cancer cells is added to fresh human blood resulting in the binding to a single nanotube

field effect transistor (FET) modified with specific antibodies by the change of electrical properties.[138]

Single-walled carbon nanotube array was developed which consisted of two columns of 10 transistors per column1 (one column was for the detection of IGF1R and the other forHer2 antibodies). The gap between the electrodes was less than ~1μm where nanotubes with lengths ranging from 1-10 μm are anchored by airbrushing. Airbrushing is a technique that uses airflow that generates torque causing a certain degree of alignment of the nanotubes along the transistors. There was an average of 10 to 12 units of monoclonal antibody (mAb) that aggregated along the length of the single wall carbon nanotubes1 (SWNT). Although the amount of single walled carbon nanotube varied, leading to different source drain currents once measured, the transistors performance on individual chips were very similar proving that the distribution of the nanotubes by airbrushing is a uniform technique[139,140] as seen in Figure 1.12. Increasing the antibody concentrations on the nanotube FET, the device performs like a P-type semiconducting FET in the sense that there was depletion in current at all the antibody concentrations tested. The depletion of current is attributed to the negatively charged antibodies, which signify that they have begun to adsorb onto the side of the SWCNT increasing resistivity and the source to drain voltage. A similar study was conducted on charge transfer to the nanotube from adsorbed proteins using small proteins such as streptavidin where in the presence of its amine group there is a donation of charge to the nanotube transistor; shifting the device characteristics.[141] The decrease in conductance could be due to electrostatic gating effect and Schottky barrier.[142] Electrostatic gating or charge transfer

occurs with two dissimilar molecules where a fraction of the charge is exchange providing a stability force for the molecular complex. Schottky barrier is similar to a p-n junction where there is a potential barrier that is formed at a metal-semiconductor junction (p-type and n-type). In this particular case, electrostatic gating is responsible for the decrease in conductance once the adsorbates such as the antibody donate a charge, affecting the electrostatic field around the nanotube.

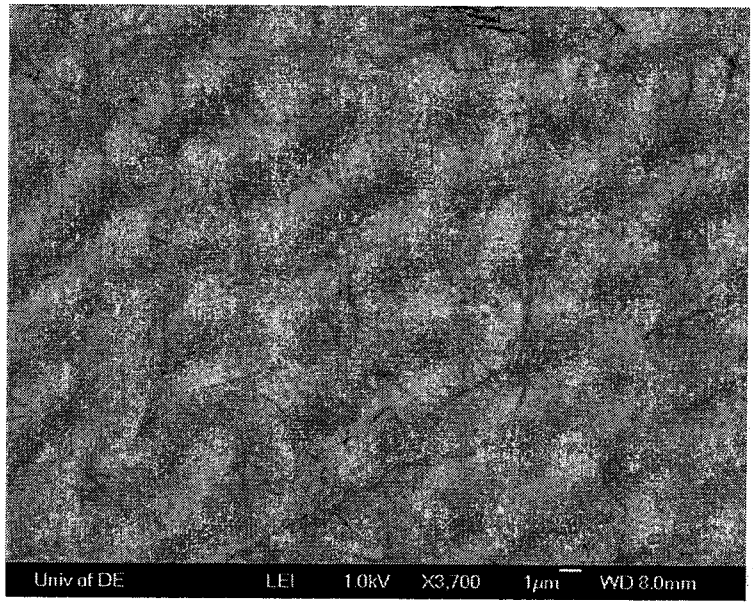

Figure 1.12. Partial alignment of single wall carbon nanotubes using air brushing. The vertical airflow generated a torque that caused the nanotubes to align (Reprinted from reference 137).

To determine if the addition of blood, which contained the proteins, will muddle up the device, a direct adsorption of the bodily fluid was allowed on the surface of the transistor array. Shao et al. reported that there was only a slight drop in current due to the spectacular design of the device, which includes the polyethylene glycol (PEG) coating

and the spacing between the electrodes; inhibiting a single cell to enter the spaces between the electrodes. The device behaves like an on-off quantum bit once the cell arrives at the electrode. The stint of current drop in the device is owed to the presence of surface electrons in the blood cells. As mentioned earlier, the device was functionalized with anti- IGF1R antibodies followed by the adsorption of MCF7 cells here they found that there was a 60% reduction in conductivity. Devices that were functionalized with nonspecific antibodies showed a 10% decrease in conductivity this was also seen for non-malignant MCF10A cells, which do not express IGF1R3.[137] According to these results it's fitting to say that conductance is greater for specific pairs than non-specific pairs or the control cells. The specific binding of antibodies to their antigens creates a change in free energy that allows aggregation; creating stress on the surface.[143-145] For the reason that the nanotubes are constrained between the electrodes inhibiting it from deflecting the binding of the cognate antibodies, it undergoes strain, changing the electron transport properties. There is an increase or decrease in the band gap associated to the tensile, compressive or torsional strain of the carbon bonds in the hexagon reducing the conductivity. The bimolecular interactions on the surface of the nanotube can be used as a "finger print" for molecular recognition or for the sensing of various types of biomolecules without labeling.

CHAPTER 2

EXPERIMENTAL

Experimental 2.1: Role of Polymer Stereoregularity on Nanocomposites of Polystyrene with Single-Walled Carbon Nanotubes

Materials. SWNT material in the form of a fibrous powder, of chirality (7, 6) and diameter range 0.7-1.3 nm was purchased from Sigma-Aldrich Co. LLC, St. Louis, MO. Syndiotactic and isotactic polystyrene was purchased from Scientific Polymer Products Inc., Ontario, NY. Syndiotactic polystyrene was received as pellets with a molecular weight (MW) of 3×10^5 g/mol and the syndiotacticity was reported as 98%. Isotactic polystyrene was obtained in powder form having an MW of 4×10^5 g/mol with a reported tacticity of greater than 90%. Atactic polystyrene was obtained from Aldrich and had a reported MW of 4.4×10^4 grams/mol. All other materials were purchased from Sigma-Aldrich and used as received.

Preparation of oxidized SWNT. SWNT was lightly oxidized by nitric acid using the method reported in literature.[176] Raman spectroscopy was used to obtain the percent oxidation of the functional tubes used in composite formation.[175, 177]

The percent oxidation was calculated according to the following equation:

$$\frac{I_D}{I_G} \times 100\%, \qquad (2)$$

where I_D is the D-band integration at 1300 cm^{-1} and I_G is the G-band integration at 1590 cm^{-1}. Comparing pristine tubes to nitric acid oxidized tubes, the degree of functionalization was found to be approximately 6%.

Preparation of the Composites: A bath-sonicated dispersion of lightly oxidized SWNTs in 45 mL centrifuged tube was centrifuged and washed in 10 mL distilled H_2O and 10 mL MeOH several times. The SWNT was re-dispersed in 20 mL of dimethyl formamide (DMF) and bath sonicated for 60 min. Separate solutions each containing 100 mg of isotactic, syndiotactic, or atactic polystyrene were dissolved in DMF, allowed to stir overnight, and sonicated for 60 min. An additional step was required for isotactic and syndiotactic PS where 2.0 g of the polymers were pre-dissolved in THF at 30°C for facile processing. To prepare the composites, each PS solution was mixed with a SWNT solution containing 0.25, 0.5, 1, 2, 3 or 5% mass of SWNTs relative to PS mass. Each sample was allowed to stir 60 min, sonicated for 60 min, and then stirred overnight. The samples were precipitated in 10-fold excess H_2O stirring vigorously, filtered using PTFE membrane, washed with H_2O and MeOH and then dried at 110°C for one hour in the vacuum oven.[175]

Carbon $T_{1\rho}$ Relaxation. Rotating frame carbon spin lattice relaxations ($T_{1\rho}$) of solid samples were determined at room temperature in 500 MHz NMR instrument at a

spinning rate of 5 kHz with 5 mm Zirconium spinner. A 4 μs 90° pulse sequence (p1) was employed followed by variable durations. Typically, the spin locking pulse sequence was applied ranging from 0.001 ms to 5 ms (16 different pulses) to the samples within the expected range of relaxation time. The value of pulse power p1 was used same as p1 (= 4 μs) for relaxation measurement purposes. The number of pulse sequences corresponded to the number of data points collected for the relaxation calculation. Relaxation data was directly fitted to a binomial equation using Bruker topspin analysis software.

Instrumentation. Ultrasonification was performed using a Fisher FS-30 160W 3QT ultrasonic cleaner. Differential scanning calorimetric analysis was conducted under nitrogen using a TA Instrument Q2000 with Tzero hermetically sealed lids and pans. Solution NMR spectra were obtained using a Bruker 500 MHz nuclear magnetic spectrometer using deuterated solvent chloroform.

Sample Preparation and Measurement. For each pure polymer sample, ^{13}C NMR spectra were obtained in deuterated chloroform at room temperature using a solution of 3-5 mg of polymer in 0.75 ml of solvent. The 500 MHz ^{1}H-NMR spectra of SWNT-polymer solutions were also carried out in chloroform (deuterated) at room temperature. The changes in chemical shift for the aromatic protons of the polystyrene as a function of SWNT were determined relative to the chloroform peak at 7.29 ppm. Each sample was run three times and the average change in chemical shift was determined. Pure polymer samples and composites were placed in DSC Tzero pans as a thin layer of powder for equal distribution. To produce good sample-pan contact, a pre-melt step was ramped up to 250°C, held for five minutes and cooled at 30°C per minute. Only 1-2 runs

were necessary to reach a limiting constant value for the T_g. For all samples, the sample sizes did not exceed 3-5 mg. Glass transition temperature and changes in heat capacity (ΔC_p) measurements were obtained using steps previously reported[175] including a heating ramp rate of 10°C/min and cooling ramp rate of 60°C/min from a fully melted sample.

2.2 Computational Methods

First-principles calculations based on dispersion-corrected DFT was employed to describe interactions between the polystyrene and SWNTs. Perdew–Burke–Ernzerhof (PBE) parametrization of exchange correlation was used with a double numerical with polarization function (DNP) basis set as implemented in DMol3.[177] The general gradient approximation (GGA) results were subsequently rectified through the inclusion of a dispersion correction effect. Tkatchenko–Scheffler (TS) dispersion correction accounts for the relative variation in dispersion coefficients of differently bonded atoms by weighting values taken from the high-quality *ab*-initio database with atomic volumes derived from partitioning the self-consistent electronic density. The TS scheme exploits the relationship between polarizability and volume. The optimization of the atomic position was performed with convergent forces less than 0.01 eV/Å. The change in the energy was less than 3×10^{-4} eV per unit cell.

Experimental 2.3: Functional Polymer Nanostructures to Control Material-Cell Interactions

Materials. Potassium metal, calcium hydride, benzophenone, styrene, ethylene oxide dicyclohexylcarboiimided (DCC), dimethylaminopyridine (DMAP) and dodecanethiol AuNPs were procured from Aldrich Chemical Company, USA. Monomers

were dried over CaH_2 and distilled prior to polymerization. Tetrahydrofuran (Fisher Scientific, USA) was purified by refluxing over fresh sodium benzophenone complex. Au(PPh3)Cl (triphenyl phosphine chloride), toluene, TWEEN-80 NaOH (sodium hydroxide), PVA (polyvinyl alcohol) were purchased from Aldrich and used as received.

Synthesis of Gold Nanoparticles by 'one-step' method. A stock solution of 1% by weight TWEEN-80 was prepared by the addition of 1 mL of TWEEN-80 to 99 mL of distilled water. Two samples were prepared using two different concentration of $KAuCl_4$. Sample 1 was prepared using a 0.4 mM concentration while sample 2 was prepared using a 0.1 mM concentration. Sample 1 was made by adding 0.4 mM of $KAuCl_4$ to 10 mL of the stock solution then transferred to a small glass vial. The solution was covered with aluminum foil to prevent any light from hitting the sample; allowing the reaction to take place in the dark at room temperature.

Preparation of Di-initiator. The di-carbanion initiator (α-methylstyrene dimer dianion, in Scheme 3.1) used for the polymer synthesis was prepared by reacting potassium mirror (5g) with α-methylstyrene (6 ml) in 200 ml THF. Under high vacuum techniques the solution turned red after shaking, indicating the formation of the di-initiator. The di-initiator was later stored under high vacuum in ampoules.

Synthesis of α, ω-bi [Biotin-poly (ethylene oxide)-b-poly (styrene)-b-poly (ethylene oxide)], (Biotin-PEO-PS-PEO-Biotin). Through an electron transfer reaction of α-methylstyrene and potassium (mirror) metal the di-initiator was created.[198] Using standard high vacuum techniques, polymerization was carried out in all-glass sealed reactors. The reactors were cleaned, annealed; and later equipped with monomers

(styrene and ethylene oxide) and initiator ampoules (with breakseals) as shown in Scheme 3.1. The reactor was attached to the vacuum line, and 10 ml THF (~10/1 solvent/ monomer, vol/vol) was distilled into the flask. Through heat-sealing with a hand torch technique, the reactor was later detached from the vacuum line and transferred to an ice bath maintained at 78°C. First, 4 ml (0.27 mmol/mL) initiator was added by breaking the breakseal of the initiator ampoule. This was then followed by the introduction of styrene (3 ml). There was a color change of the solution from clear to deep red, indicating the formation of polystyrene anion. Ethylene oxide (1mL) was added to the solution after the reaction was allowed to proceed for 40 minutes. The color disappeared completely after a few minutes signifying the initiation of the second monomer. For two days at room temperature while the second monomer (ethylene oxide) was allowed to ensue before terminating with the addition of methanol and hydrochloric acid to produce the α, ω-dihydroxyl polymer [HO-PEO-PS-PEO-OH]. The functional polymers were purified by precipitation into hexanes. Yields were >90%. Reaction of the α,ω-dihydroxyl polymer with biotin in the presence of *N, N'*- dicyclohexylcarboiimide (DCC) and dimethylaminopyridine (DMAP) resulted in the formation of *α, ω-bi* [Biotin-poly (ethylene oxide)-b-poly(styrene)-b-poly(ethylene oxide) (Biotin-PEO-PS-PEO-Biotin). To purify the product, the excess biotin was removed using a separatory method. Sodium bicarbonate was added to the round bottom flask containing the product forming a thick white slurry. The slurry was then transferred to a separatory funnel where methylene chloride was later added. The contents in the flask were then agitated forming a mixture. After allowing the contents to settle for 15 minutes, two distinct layers formed. The lower

layer containing the pure functionalized polymer was extracted leaving behind the top layer. The top layer was comprised of biotin salts which was formed from the excess biotin.

Scheme 2.1. Synthesis of α, ω-bi [poly (ethylene oxide)-b-poly (styrene)-b-poly (ethylene oxide)], Biotin-PEO-PS-PEO-Biotin

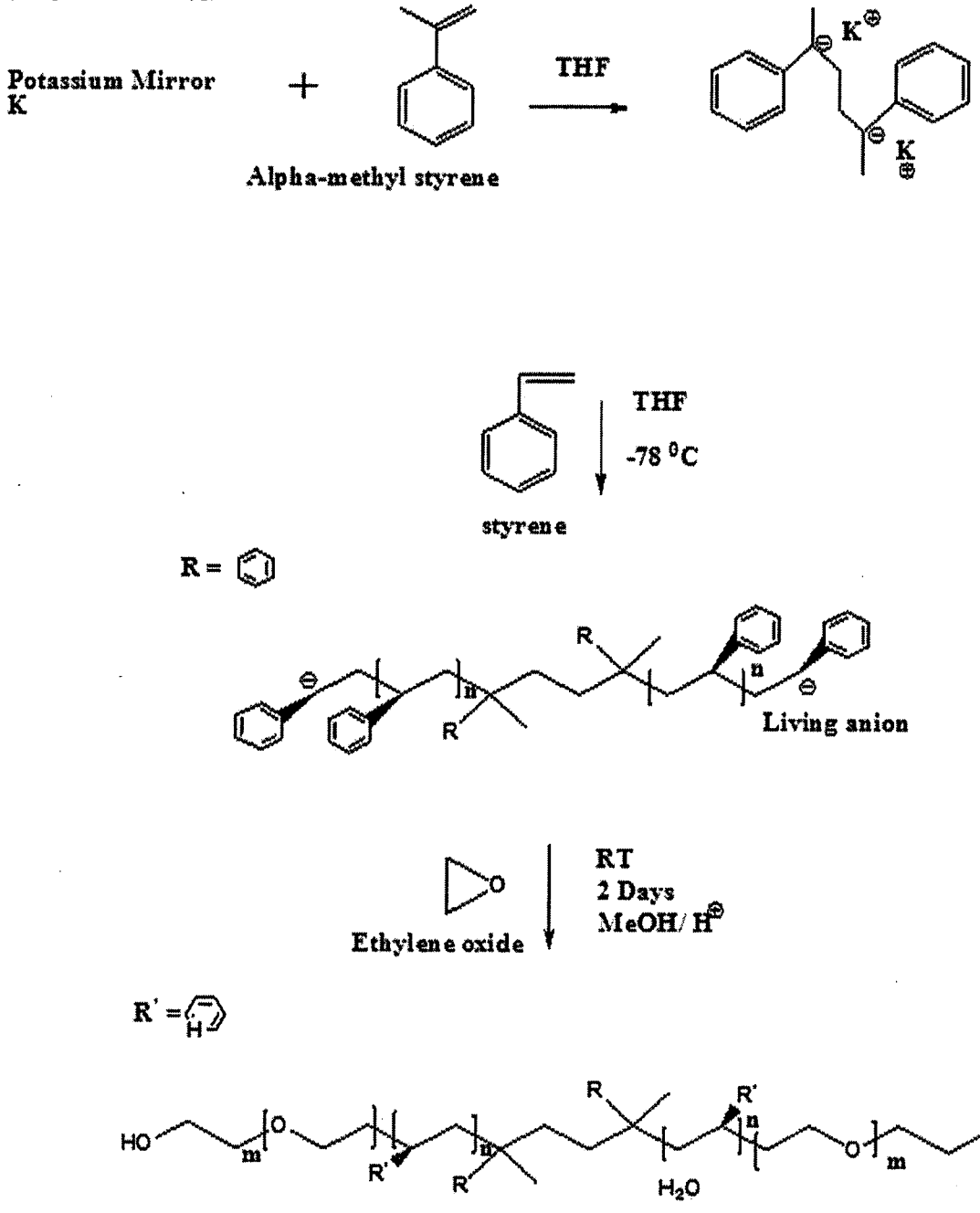

2.4 Electrospinning of polymers

Biotin-PEO-PS-PEO-Biotin Fibers. *Biotin-PEO-PS-PEO-Biotin* polymer and dodecanethiol AuNPs were mixed in a 1:1 and 1:2 ratio with high molecular weight polystyrene (1,000,000) in DMF forming a 10 wt% solution.

PVA/AuNP Fibers. PVA was prepared using a 21 wt. % solution in a 50 mL flask using 10.5mL of the gold solution synthesized by the one-step method and 10.5mL of ethanol via the slow addition of 5.05 g PVA. The opening of the flask was sealed using *parafilm* to prevent any solvent loss due to evaporation as the mixture was stirred and heated at of 40°C for 20 mins. The substrates on which the fibers were collected are silicon, indium tin oxide (ITO) coated polyethylene terephthalate (PET), fluorine tin oxide (FTO) coated glass, and glass.

Electrospinning of the polymers were carried out where the polymer solution is forced through a capillary tube attached to a syringe forming a drop at the end of the needle. A voltage is applied to the tip of the needed and the grounded collection target. The strength of the electric field overcomes the surface tension of the droplet forcing a polymer solution jet to collect at the grounded collection plate. As the jet travels through air towards the grounded region the solvents evaporates leaving a nonwoven polymeric fiber behind.

2.5 Analysis and Measurements

Size exclusion chromatography (SEC) was performed using a Perkin Elmer Binary LC pump 250, a 2792 injector and Perkin Elmer LC-30 RI detector. Three columns, HR3, HR 4E, HR 5E, were used in conjunction with 2μm precolumn filter. The

columns were housed in an oven maintained at 30 ^{0}C. Tetrahydrofuran was used as the eluent at a flow rate of 1 ml/ min. Molecular weights were calculated relative to polystyrene (Aldrich) molecular weight standards.

^{1}H NMR spectra were obtained using a Bruker ARX 500 NMR spectrometer in $CDCl_3$ and DMF-d_8. Trimethylsiloxane was used as internal standard. FTIR spectra were recorded on a Perkin Ekmer Spectrum-65 FTIR spectrometer with an accuracy band of ± 2 cm^{-1}. Differential scanning calorimetry was performed on a TA Instrument Q2000 at a heating rate of 10°C per minute, and the reported values were obtained from the third heating after quench cooling the sample. The T_g's were taken at the midpoints of the heat capacity changes, the T_m's were taken at the maximum of the enthalpy endothermic peaks. The DSC was calibrated for temperature and enthalpy using an indium standard under nitrogen gas atmosphere. X-ray photoelectron spectroscopy (XPS) spectra were obtained using a Thermo K-Alpha XPS.

CHAPTER 3

RESULTS AND DISCUSSION

Part 1: Role of Polymer Stereoregularity on Nanocomposites of Polystyrene with Single-Walled Carbon Nanotubes

3.1 Discussion

The study of nanocomposites composed of single-walled carbon nanotubes (SWNT) and polymers is an exciting area of materials research.[155-160] The interest in SWNTs as the nanofillers is attributed to their unique mechanical and electrical properties. Additionally, the high aspect ratio of SWNTs permits desired property enhancements at very low concentrations. For effective property enhancements at low concentrations, the SWNTs need to be individually dispersed within the composite matrix. Electrically conductive composites with excellent properties have been obtained with SWNT loadings lower than 1 wt%.[161-164] However, SWNTs normally agglomerate into bundles within polymer matrices and thus to individually disperse the SWNTs, requires effective SWNT-polymer interactions.[165-168]

Several studies on SWNT/polymer nanocomposites have investigated the effect of varying the type of components, e.g., molecular weight of polymers, different polymer types such as block copolymer, nanofiller shape and size. However, to the best of our knowledge, the role of polymer stereoregularity on the formation of nanocomposites has not been studied. Polymer stereoregularity is a fundamental three-dimensional structure

of most vinyl polymers. Stereoregularity can have a profound effect on the conformation of polymers and their physical properties.[169-172] For example, syndiotactic poly(methylmethacrylate) has a glass transition temperature of 105 ^{0}C and that of the isotactic polymer is around 40°C.[173] Therefore, it is important to understand the role of polymer stereoregularity on nanocomposite formation. This study is particularly relevant, because the dimensions are on a size scale where changes in stereoregularity and conformation may affect the nature of the interaction between the polymer and the SWNT.

Nanocomposites composed of SWNT and polystyrene (PS) have been reported by several groups.[161, 174-175] The studies have led to an understanding of the interaction between the SWNT and polystyrene as a function of molecular weights, weight fraction of SWNT in the composites, and different processing methods. However, none of the studies considered the stereoregularity of polystyrene. The previous studies most likely utilized the most common form of polystyrene, which is the atactic polystyrene. The atactic polystyrene has approximately equal meso (isotactic-like) and racemo (syndiotactic-like) dyads in the polymer. Furthermore, the meso and the racemo dyads are randomly distributed in the polymer chain. The three-dimensional spatial orientations of the meso and racemo dyads are shown in Figure 3.1. In a purely isotactic and a purely syndiotactic polymer one hundred percent of the dyads are meso and racemo, respectively.

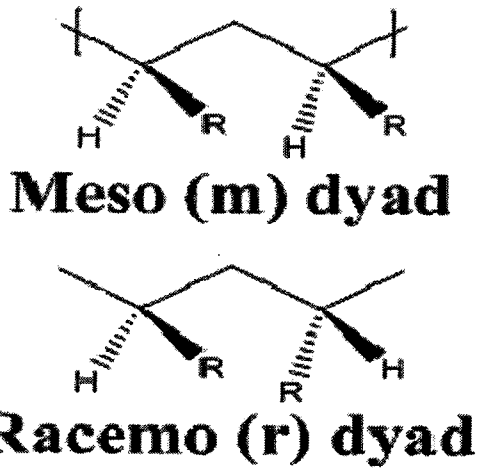

Figure 3.1. Meso and racemo dyads.

Polystyrene was selected as the matrix polymer in this study, because it has been extensively studied with respect to its stereoregularity and chain conformations. Isotactic polystyrene forms a helical conformation in the solid state.[176] The helical conformation is either in the extended helical conformation with a non-staggered trans-trans conformation or three fold helical trans-gauche conformation. The conformation of isotactic polystyrene in the solid state is substantially different from the atactic polystyrene. Tchoul *et. al*[161] conducted a study on the preparation and evaluation of the electrical conductivity of SWNT-polystyrene composites. The study revealed that dispersion of the nanotubes was significantly affected by SWNT functionalization, resulting in dramatic shifts in the percolation threshold of conductivity. Grady *et. al.*[175] conducted a study on how oxidized SWNT nanofillers change the dynamics of polystyrene around the glass transition. They concluded that at a high SWNT content, there was an increase in the

change in the heat capacity at the glass transition; hence the SWNTs were participating in the molecular motion.

The report on a combined experimental and theoretical study of SWNT/polystyrene nanocomposite is discussed here. Theoretically the employment of force field based molecular dynamics and density-functional calculations were carried out to understand the effect of stereoregularity of the polymer on the formation of the nanocomposite. In particular, in this report we have carefully compared the isotactic polystyrene/SWNT composite with the atactic polystyrene/SWNT composite. The relevancy of the computational results have been examined and tested with experimental data obtained by DSC and NMR methods.

3.2 Results

The present work utilizes a combination of force-field based molecular dynamics and density-functional calculations, as well as experimental approaches to investigate the effect of stereoregularity of polystyrene on SWNT/polystyrene nanocomposite formation. Calculations were performed on purely isotactic, atactic and syndiotactic polystyrene to determine which polymer has the stronger affinity for interacting with the surface of the SWNT. Each model was composed of twelve monomer units. The isotactic and syndiotactic models consisted of purely all meso or racemo dyads, respectively (Figure 3.1). The atactic polystyrene has a random distribution of meso and racemo dyads. The dispersion of the SWNTs within the different polystyrene (isotactic, atactic, and syndiotactic) matrices was studied by solution and solid-state state NMR spectroscopy, and differential scanning calorimetry (DSC). The surface of SWNT is hydrophobic and

inert in nature. These properties were not favorable for producing a polymer nanocomposite with the SWNT as nanofillers.[175] In order to improve the interaction of SWNT with the polystyrene, the SWNTs were functionalized using nitric acid oxidation.[176]

Theoretical computations demonstrate that the semi-rigid aromatic polymer backbone has certain flexibility to adjust its conformation during successive helical wrapping. The first sets of calculations were carried out using pristine SWNTs. Among the three tacticities shown in Figure 3.2, it was observed that isotactic polystyrene forms the lowest energy complex. The calculated binding energies listed in Table 3.1 revealed atactic/SWNT as the second most stable complex and the syndiotactic polystyrene/SWNT as the least stable. The oxidation of SWNT further stabilized interaction of both isotactic and the atactic polystyrene with the SWNT, while the binding between the syndiotactic and the SWNT remains the same. Oxidation increases the polarity of the SWNT resulting in an increase in the dipole-dipole interaction of the phenyl protons of polystyrene and the oxidized groups on the SWNTs. The binding energy data suggest that the isotactic polystyrene is more effective in interacting with the SWNT. This is very interesting, because the only difference between the isotactic and the atactic polymers is the spatial orientation of the repeat units. The stereoregularity in turn plays a role in the overall polymer conformation. Therefore, a plausible explanation may be that because the isotactic polystyrene forms an extended helical conformation, it may be in the most favorable orientation to wrap around SWNTs.

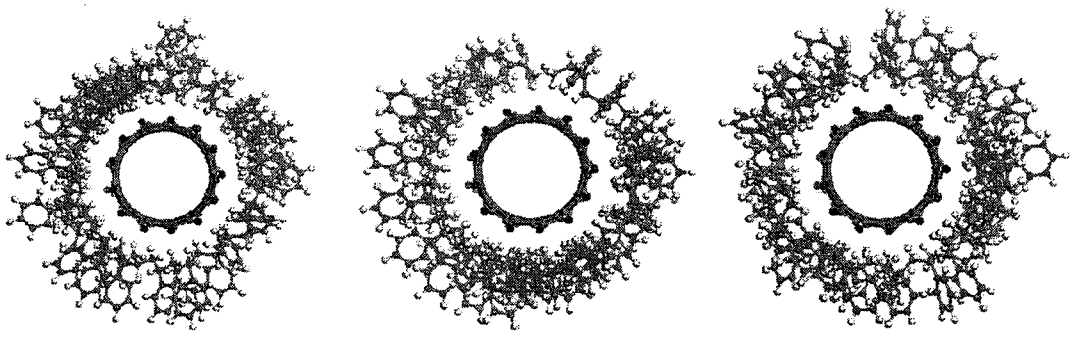

Figure 3.2. Predicted conformation for the complexes of polystyrene and SWNTs.

Table 3.1. Calculated Binding Energies Among the Three Tacticities of Polystyrene

Tacticity	(BE) oxidized SWNT (kcal/mol)	(BE) pristine SWNT (kcal/mol)
Isotactic	-237.09	-236.83
Atactic	-229.10	-228.97
Syndiotactic	-228.12	-228.12

Polystyrene Stereoregularity. The stereoregularity of the polymers were determined by ^{13}C NMR spectroscopy. The 500 MHz ^{13}C NMR spectra of the quaternary carbon of the isotactic and atactic polystyrenes are shown in Figure 3.3. The isotactic polymer displays one strong peak at 146.2 ppm and the atactic polymers displays five

peaks indicating pentad resolution. The peak at 146.2 observed for the isotactic polystyrene is assigned as the mmmm pentad. Considering that there is only a single peak observed for the quaternary carbon, the polymer is almost 100% isotactic.

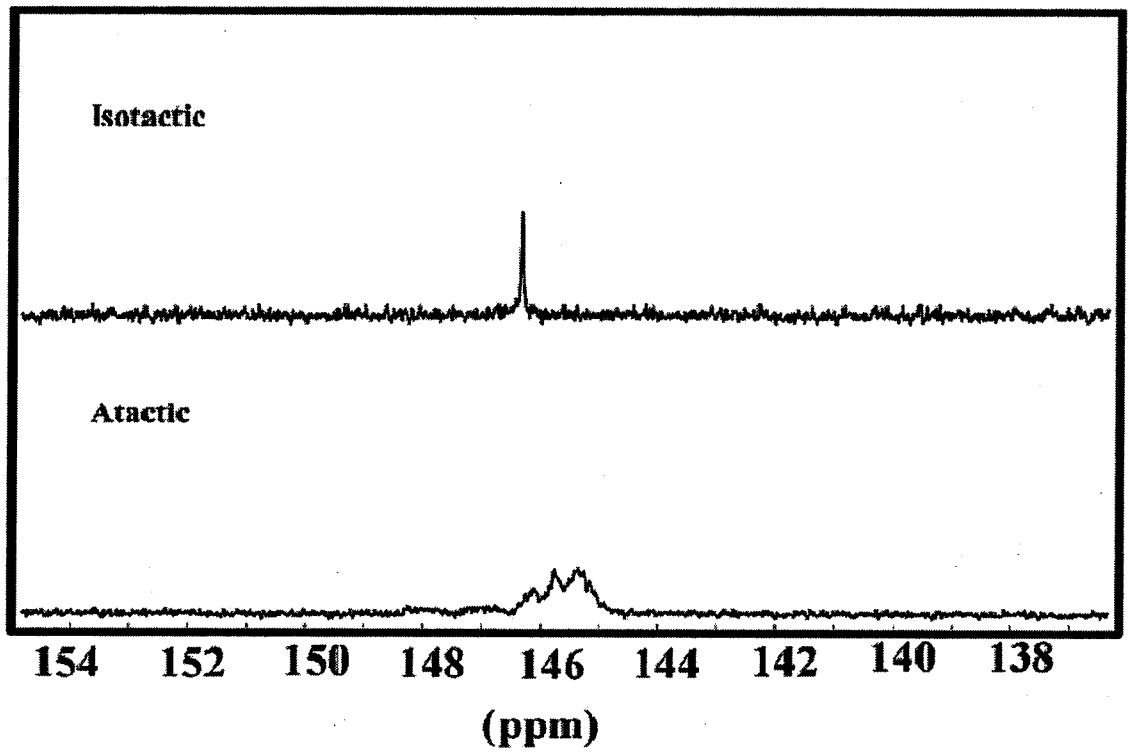

Figure 3.3. ^{13}C NMR spectra of the quaternary carbons of the isotactic and atactic polystyrenes.

The pentad stereochemical assignments for the atactic polymer are shown in Figure 3.4. The assignments were obtained by deconvolution of the quaternary peak shown in Figure 3.3. These assignments were made by comparison with the isotactic polymer and previously published stereochemical assignments.[178] The peak at 146.2 ppm was assigned to the mmmm pentad and the other four observed peak regions were

assigned to pentads as listed in Table 3.2. Furthermore, the observed pentad intensities for the atactic polymer matched well with Bernoulli calculations, also listed in Table 3.2.[179] The Bernoulli calculations were carried out using *Pr* value of 0.4. The *Pr* value was determined using the quaternary carbon mmmm pentad of the atactic polymer. The NMR analysis confirms the isotacticity and atacticity of the two polymers used in this study.

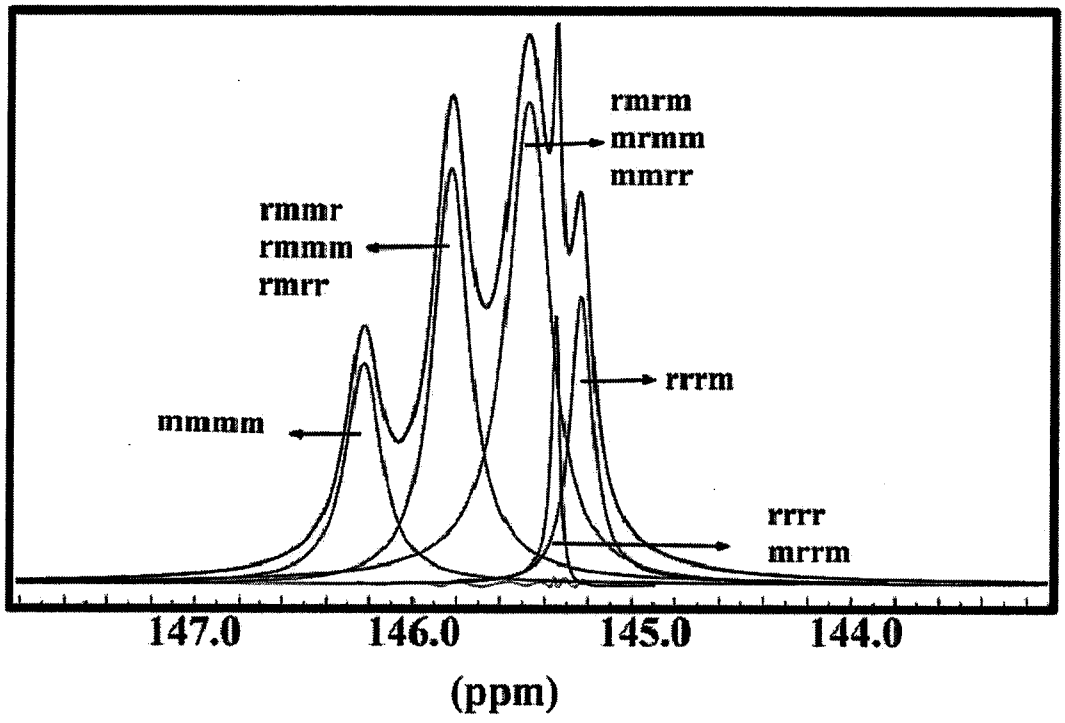

Figure 3.4. Pentad assignments of quaternary carbon peaks obtained by deconvolution.

Table 3.2. Stereochemical Assignments of Atactic Pentad Peaks

Peak Reg.	Chem. Shift (ppm)	Assignment	Observed Quaternary	^{1}r=0.40
A	146.2	mmmm	0.14	0.13
B	145.8	rmmr	0.29	0.31
		rmmm		
		rmrr		
C	145.5	rmrm	0.42	0.4
		mrmm		
		mmrr		
D	145.3	rrrm	0.04	0.8
E	145.2	rrrr	0.11	0.8
		mrrm		

Thermal Studies. The glass transition temperatures of the pure polymers and the polystyrene/SWNT nanocomposites are listed in Table 3.3. The DSC thermograms of isotactic polystyrene/SWNT nanocomposites are shown in Figure 3.5. The observed T_g values of the pure atactic-PS, syndiotactic-PS, and isotactic-PS were in good agreement with previously reported values of ~100, ~95, and ~90°C, respectively.[178]

The glass transition temperature of the atactic polystyrene decrease initially and reaches a plateau with 0.5% weight SWNT content. This observation is in conformity with the observation of Koning *et. al.* that there is a slight decrease in T_g for PS-SWNT composites.[180] The slight decrease is attributed to the initial plasticization of the polymer by the SWNTs.

Table 3.3. Glass transition Temperature (T_g) of the Pure Polymers and the Polystyrene/SWNT Nanocomposites.

% SWNT	Atactic (°C)	Isotactic (°C)	Syndiotactic (°C)
0	102.9	90.9	97.8
0.25	98.3	98.4	-
0.5	99.8	100.5	100.2
1	99.5	100.2	100
2	98.9	100.8	99.8
3	100.1	99.9	99.9
5	99.8	100.4	98.3

With additional SWNT, larger agglomerates form, without affecting the segmental motion of the polymer chains. These agglomerates can be viewed as small distinct domains, which do not affect chain mobility. The isotactic polystyrene shows quite different thermal behavior. As the SWNT content is increased in the isotactic polymer, an increase in the T_g of the isotactic polystyrene/SWNT composite is observed. The glass transition temperature increases from 91°C to 100.5°C as the SWNT content is increased to 0.5%. Further increase in the SWNT content does not change the T_g. The glass transition temperatures of the syndiotactic polystyrene composites are also relatively unaffected on increasing SWNT. The T_g of the syndiotactic polystyrene slightly increases to 100°C at 0.5 %SWNT content and further increase does not affect the glass transition temperature. The magnitude of ΔC_p at the glass transition temperature for the isotactic polystyrene/SWNT composites increases as the SWNT content is increased. For the pure isotactic polystyrene the ΔC_p is 0.27 J/g°C. As the SWNT content is increased in the isotactic composite, the ΔC_p increases with increasing SWNT content and reaches a value of 0.43 J/g°C at 1% by weight SWNT (Figure 3.6). The increasing change in the change in the heat capacity suggests that at the glass transition temperature segmental motion involves polymer chains complexed with the SWNT in the isotactic composite.

The increase in glass transition temperature and in the change in heat capacity indicates that the isotactic polymer has the best ability to interact with the SWNT in the nanocomposite. Therefore, both computational and experimental results suggest that the

isotactic polystyrene is most effective in interacting with the SWNT. The pictorial depiction of the addition of the SWNT to polystyrene (Scheme 3.1). As SWNT is added to the polymer, if the polymer has the ability to interact well with the SWNT, SWNT/polymer complexes are formed as depicted in Type A matrix. The complexation of the polymer with the SWNT results in the formation of a psuedo-crosslinked matrix leading to an increase in the glass transition temperature.

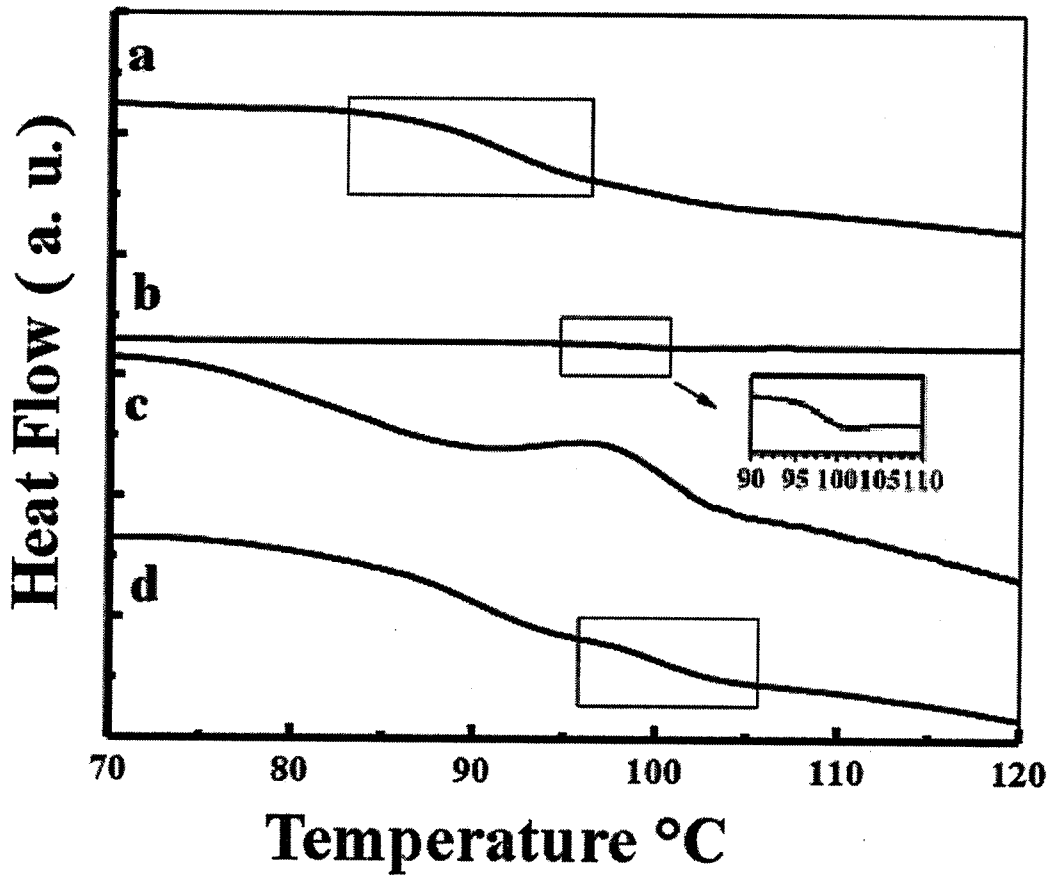

Figure 3.5. DSC thermograms of isotactic polystyrene/SWNT nanocomposites. a. pure isotactic polystyrene, b. 0.25 % SWNT, c. 1 % SWNT, d. 0.5 % SWNT.

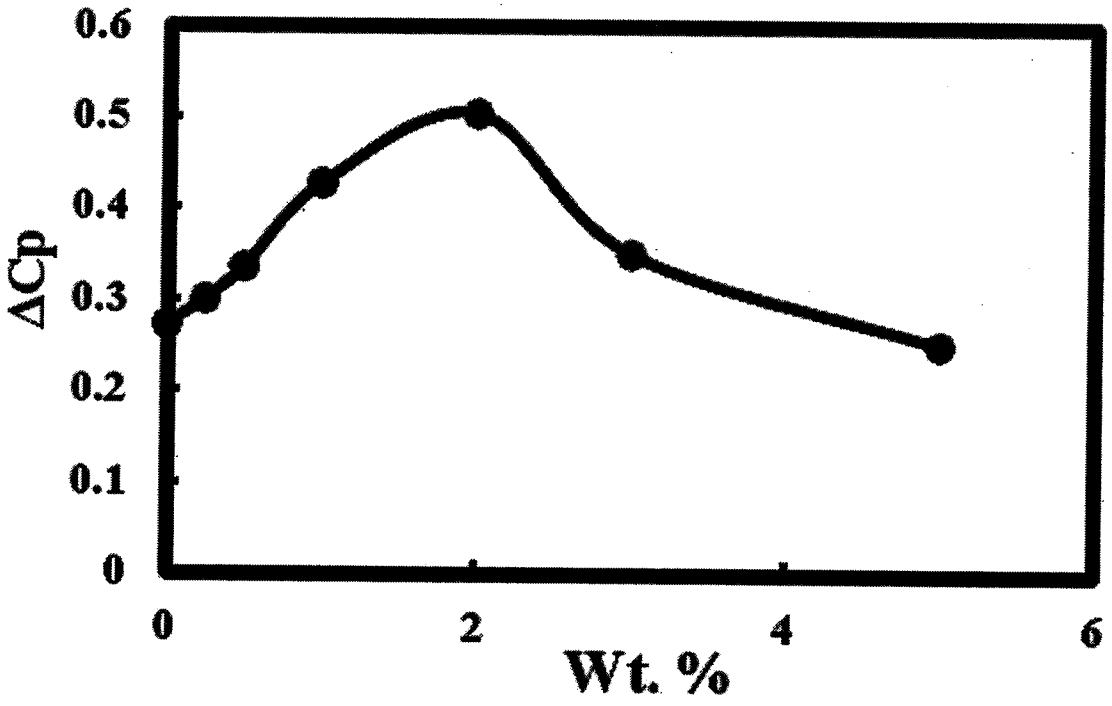

Figure 3.6. The ΔC_p of isotactic polystyrene/SWNT nanocomposite as a function of nanotube content.

In the isotactic polymer/SWNT matrix two or three polymer chains perhaps interact with one SWNT resulting in pseudo-crosslinking. This type of pseudo crosslinking is observed in certain polymer/salt systems[181-182] because of ion-dipole interactions. Further addition of SWNT to Type A matrix results in agglomeration of the SWNT as the capacity of the polymer to interact or complex with the nanofiller is saturated. Any additional SWNT past this point agglomerates and can be depicted as shown in Type B matrix. Therefore, the additional SWNT, greater than past 0.5 wt.% to 5 wt.%, simply forms agglomerates which do not interact with the polymer chains.

Therefore the glass transition temperature is unchanged. This is exactly the observation for the isotactic polystyrene/SWNT composite. If the polymer does not interact well or complex effectively with the SWNT, even at low SWNT contents, the SWNT will mostly likely start aggregating and Type C matrix will form. Therefore, a plasticization effect may be observed at low SWNT content. Further, increase in SWNT will result in agglomeration and hence after the initial plasticization, the glass transition will not be affected. This type of behavior is observed for atactic polystyrene/SWNT composite. From the thermal studies, one can conclude that the isotactic polystyrene interacts better and is effective in complexing with the SWNTs compared with the atactic polystyrene.

Scheme 3.1. Depiction of the Three SWNT/Polymer Matrices.

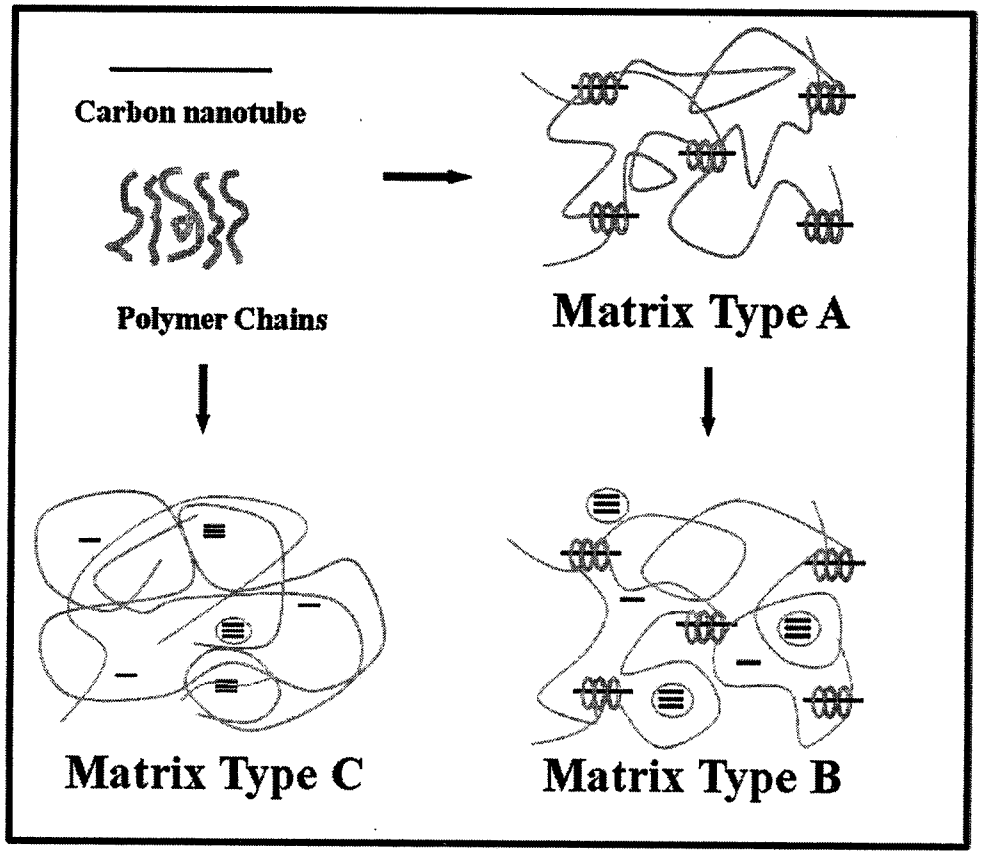

Solution and Solid State NMR studies. The band structures for the isotactic and the atactic polystyrene wrapped SWNT are shown in Figure 3.7. The computational results show that the phenyl group of the polystyrene is the donor, and such donation should results in a decrease in the π-electron density of the aromatic ring. This decrease in the π-electron density may result in de-shielding of the aromatic protons as the aromatic protons may shift downfield.[183] Computational studies suggest charge transfer interaction between the polymers with the SWNT. The flat bands represent the non-interacting (non-dispersed) polystyrene polymer molecular levels with SWNT. As a result of the charge transfer from the polymer to the SWNT, flat bands near Fermi level disperse. In the isotactic band structure (Figure 3.7), the flat band has lower energy than the atactic band structure. The flat band regions are highlighted by brackets in Figure 3.7. This indicates that there are more polymer molecular levels interacting with SWNT in isotactic polystyrene compared to atactic polystyrene. The isotactic polymer is a better charge donor to the SWNT compared to the atactic polymer. It has been shown earlier that in a poly(2-methoxystyrene)/graphene composite, the polymer backbone serves as charge donors to graphene resulting in the doping of graphene.[184]

The 500 MHz ^{1}H-NMR spectra of SWNT-polymer chloroform (deuterated) solutions show changes in chemical shifts as a function of increasing SWNT. The observed changes in chemical shift as a function of SWNT are shown in Figure 3.8. The change in chemical shifts (δ) was detected with respect to the chloroform peak at 7.29 ppm. As the SWNT content is increased in the isotactic polystyrene solution, a slight downfield movement of the aromatic protons is initially observed. However, when the SWNT content is 1%, the protons shifts upfield. A similar plot is also shown for the

atactic polymer, which only shows upfield shifts. The observed trends were consistent with the computational and DSC results. The downfield shift of the isotactic polymer is fairly small but these are in the solution state where one may have association and dissociation of the polymer and the SWNT taking place. But the fact that a downfield shift is observed even in solution suggests that isotactic polystyrene is better able to complex with the SWNT and act as a charge donor. The downfield shift reaches a maximum at around 0.5% SWNT. It is interesting to note that at 1% SWNT content, both the isotactic and the atactic polymers show the same upfield chemical shift. When the capacity of the isotactic polymer is saturated, any additional SWNT will agglomerate and the two systems will become quite similar in that the majority of the SWNT are in the agglomerated form.

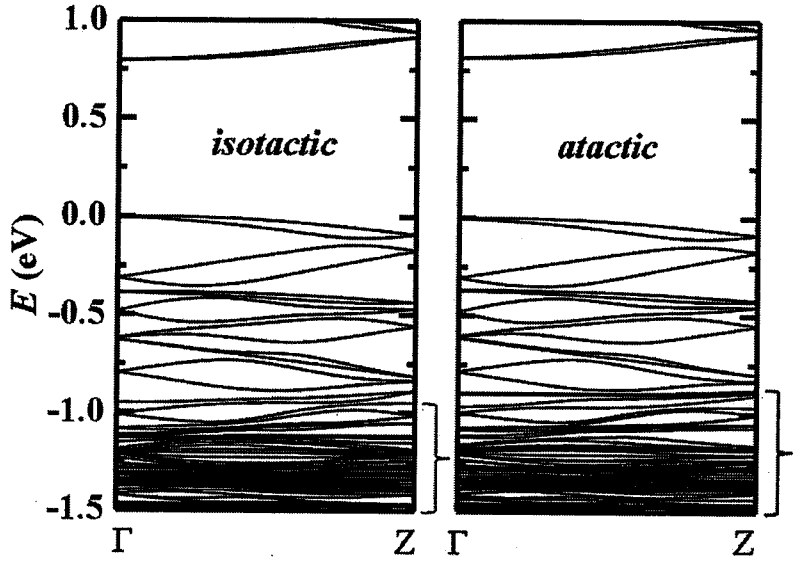

Figure 3.7. Calculated band structures for (a) *isotactic*-polystyrene wrapped swnt, (b) *atactic*-polystyrene wrapped SWNT. Γ = (0) and Z = ($\pi/2a$), where a = 47.5 Å. The valence band maximum is set to 0 eV. Brakets indicates the flat band regions of the band structure.

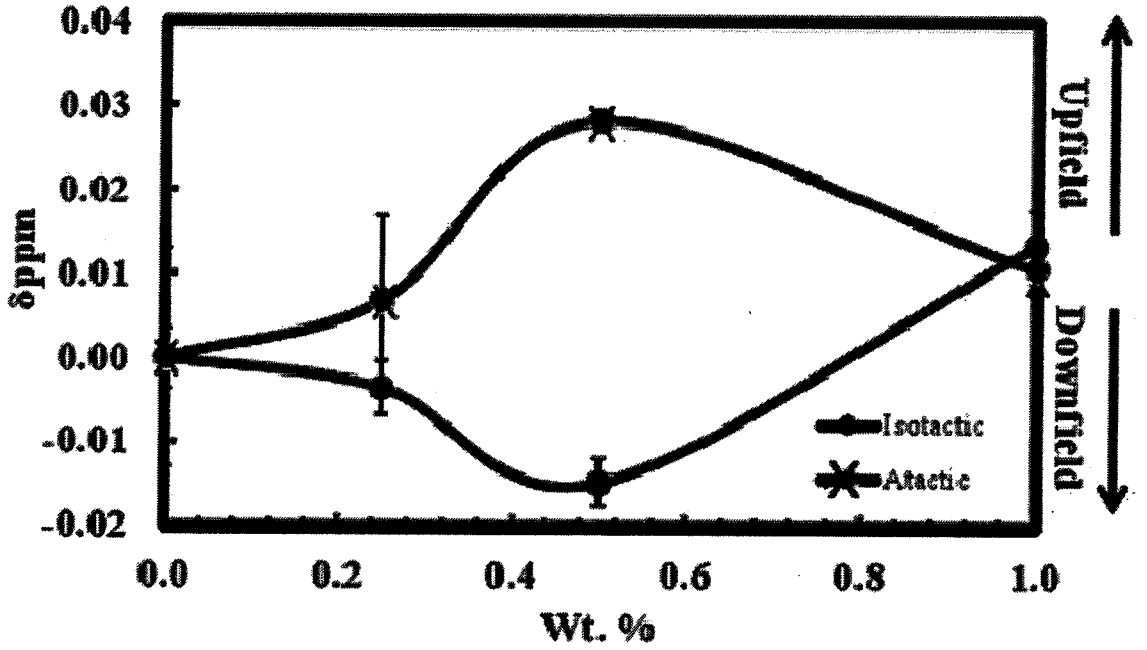

Figure 3.8. Change in chemical shift (δ) for the aromatic protons of polystyrene as a function of SWNT content.

Rotating frame ^{13}C $T_{1\rho}$ spin lattice relaxation on the nanocomposites complements the computational, thermal (DSC) and solution NMR studies. The ^{13}C $T_{1\rho}$ values are listed in Table 3.4. The spin lattice relaxation of the isotactic polymer increases on increasing the SWNT content at 1 wt%. Increasing the SWNT content in the isotactic polymer, yields an increase in ^{13}C $T_{1\rho}$. The increase in the relaxation time is most likely due to the formation of the pseudo crosslinking in the isotactic system and the decrease in the relaxation time for the atactic polymer is consistent with initial plasticization on addition of the SWNT.

Table 3.4. ^{13}C $T_{1\rho}$ Spin Lattice Relaxation of Isotactic and Atactic Polystyrene/SWNT Composites

% SWNT	Atactic (ms)	Isotactic (ms)
0	2.50	2.15
0.25	2.10	2.19
0.5	2.09	2.26
1	1.60	2.43

Computational, thermal ($T_g$and changes in heat capacity), solution and solid state NMR results strongly suggest that the isotactic polystyrene is better in dispersing SWNT within its matrix compared with the atactic polymer.

Part 2: Functional Polymer Nanostructures to Control Material-Cell Interactions

3.3 Discussion

Proteins, peptides and antibodies bioconjugates are effective in biomedical applications and have commercial success.[185] The synthesis and characterization of bio-functional polymers capable of mediating cellular responses are of considerable importance. Moreover, these polymer systems may provide an effective way of developing a broadly applicable antibody detection technique providing that the

bioconjugates remain bioactive and bioavailable after conjugation. A previous study carried out by Panyam et al. reported a simple Interfacial-Activity Assisted Surface Functionalization (IAASF) technique to fabricate ligand functionalized polymeric nanoparticles for targeted delivery.[186] In this one step synthesis, the incorporation of multifunctional groups, including hydrophilic polymers and targeting ligands, were introduced onto drug-loaded nanoparticles. Dual-ligand functionalized nanoparticles with folic acid and biotin were evaluated for specific targeting of an anticancer drug to tumors, which resulted in a high accumulation of the drug in affected tissues.

Bio-functional synthetic polymers covalently conjugated with antibodies capable of binding to their antigen can serve as a useful model system for sensors. In several cellular systems, such as, the mast cell as well as in B and T cells, small synthetic ligands had been used to investigate various receptor mediated signaling.[187,188] Attachment of a specific group to a polymeric backbone is a useful method for controlling the size, solubility and biocompatibility without eliminating biological activity.[189] A recent study shows that α,ω-bi-[2,4-dinitrophenyl (DNP)], a synthetic polymer ligand, is capable of intramolecularly crosslinking with the IgE receptor complex, inhibiting cellular activation of the immune response system in mast cells.[190]

Polystyrene has been shown to be biocompatible when used in thermoplastic elastomer blends[191] therefore, the synthesis of α, ω-bi[Biotin]-poly (ethylene oxide)-b-poly(styrene)-b-poly(ethylene oxide) ligands was carried out using di-functional anionic initiators. The present study was undertaken to develop new functional polymers that are capable of conjugation to a range of biomarkers, i.e., proteins, unlike that of the synthetic

pendant group used in the 2, 4 Di-nitrophenyl synthetic ligand study. The interaction of biotin and avidin as a ligand-receptor pair is commonly used in the field of biology and medicine for purification, localization and diagnostics, serving as a well-defined model system to probe bioavailability.[192, 193] Biotinylated polymer systems with various molecular weights have been used as model systems to study and mimic the multivalent interactions that occur during protein-cell recognition.

Functional Nanostructures. Functional nanostructures have a wide variety of applications such as medical, filtration, barrier, wipes, personal care, composite, garments, insulation and energy storage. Adding nanoparticulates to a polymer matrix can substantially enhance its performance by gaining the properties of the filler. Metal nanoparticles (MNPs) optimal (or dielectric) constants resemble those of the bulk metal to exceedingly small dimensions.[194] Metal particles (MP) exhibit strong plasmon resonance extinction bands in the visible spectrum. Yet, while the spectra of molecules (and semiconductor particle) can be understood only in terms of quantum mechanics, the plasmon resonance bands of nanoscopic metal particle can often be rationalized in terms of classical free-electron theory and simple electrostatic limit models for particle polarizability.[195] The composition of an MNP may be held constant as its plasmon resonance can be shifted hundreds of nanometers. Adding an external stimulus such as temperature changes its shape and or orientation in the incident field. Metal particles are ideal, because they can be synthesized and modified chemically due to their similarity to continuous metal surfaces.

One-dimensional nanostructures, such as, nanofibers have a wide range of technological applications in electronic, photonic, catalytic, biomedical and water

purification industries.[196, 197] Nanofibers exhibit special properties mainly due to their extremely high surface to volume ratio compared to conventional nonwovens. Electrospinning is one approach to preparing these nanostructures. The process includes the forcing of polymeric material through a capillary tube forming a droplet at the needle's end. An electrical potential is then applied to the tip of the capillary tube causing the strength of the electric field to overcome the surface tension of the droplet leading to the creation of nonwoven fibers at the grounded collection plate region. Processing conditions or parameters including voltage, federate, temperature, needle tip diameter and the distance between the tip and the collector plate can affect the properties of the fibers formed.

The preparation of electrospun functional nanofibers and gold nanoparticles (AuNP) is reported. A preliminary study on nanofiber formation using polyvinyl alcohol is also discussed.

3.4 Results

PVA/AuNPs Nanostructures. Several characterization techniques were used in order to analyze the properties of the synthesized gold nanoparticles and the composite gold/PVA nanofibers. These characterization tools included refractometry, UV-Visible spectrometry, as well as a transmission and scanning Microscopy. During the reaction of the one-step gold nanoparticle synthesis the refractive index was measured at thirty-minute intervals using a refractometer. The refractive index increased over time with most of the growth occurring after 5 hours as displayed in Figure 3.9.

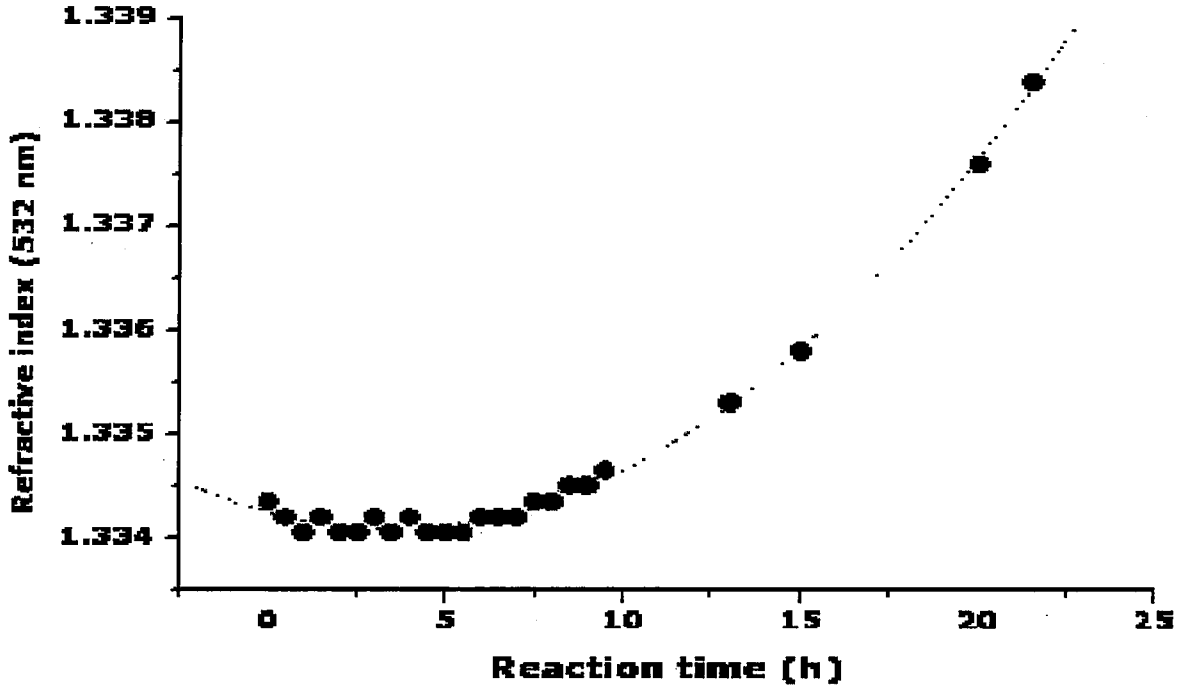

Figure 3.9. Time evolution of the refractive index

A UV-Vis scan taken at twenty-minute intervals throughout the reaction shows the decrease in absorbance around 300 nm while there was a significant increase in peak intensity at 650 nm (Figure 3.10). This is expected because as the reaction progresses the solution changes color from yellow to red. It was observed that the color change occurred most rapidly between hours two and three of the reaction, indicating that this is the time when most of the gold nanoparticles were formed. To further understand the mechanism in which this reaction takes place, the change in absorption via UV-Vis and refractive index was taken every five minutes. A future goal is to find the correlation between the change in refractive index and the change in absorption during this time period.

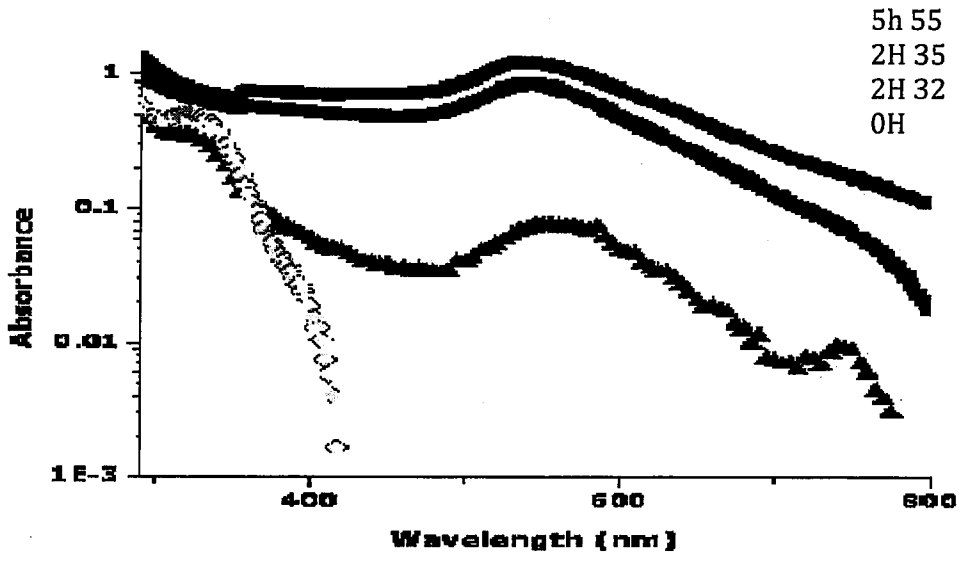

Figure 3.10. Uv-Vis: Time evolution of the absorbance peak of Au nano-clusters/nano-particles.

Physical observation shows that some residual gold nanoparticles were floating freely in solution, but the majority of the particles were settled at the bottom of the flasks. The gold nanoparticles ranged in diameter from approximately 3 - 43 nm using TEM. It was also observed that some of the gold nanoparticles formed perfect polygons as shown in Figure 3.11. The figures that show the gold nanoparticles from the interface synthesis show an even spacing amongst the nanoparticles, from which it can be inferred that there is some type of non-covalent bonding occurring among the nanoparticles. Using TEM the PVA/AuNPs fibers were imaged (Figure 3.12). There are few gold nanoparticles mixed within the PVA nanofibers. One reason for the lack of distribution of nanoparticles throughout the matrix is due to the non-functionalization of the particles

with thiol groups. The addition of a thiol group would allow for anchoring of the NPs to the polymer matrix along with the prevention of agglomeration.

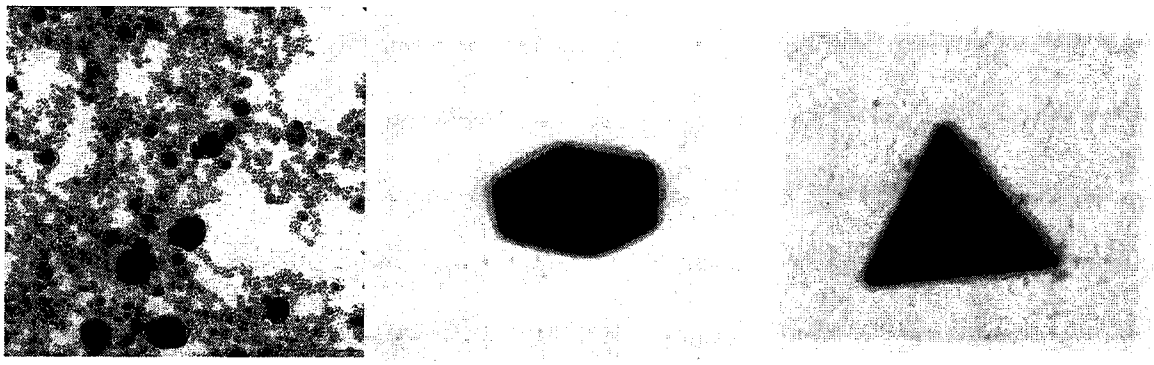

Figure 3.11. Au Nanoparticles with triangular and pentagonal shapes

Figure 3.12. TEM image of PVA/AuNPs composite

A scanning electron microscope (SEM) was used to study the surface morphology of the gold/PVA nanofibers that had been electrospun on to several different substrates as a function of time. The SEM indicated that there was very little alignment of the fibers. In Figure 3.13, the ITO coated in PET and the aluminum showed almost no alignment of the fibers; however, the fibers electrospun on the silicon substrate showed some alignment towards the edges. Alignment was achieved because the silicon substrate is conductive. The fibers also appeared to be larger in diameter than desired (<100nm). Increasing the voltage may help to minimize the diameters of the fibers.

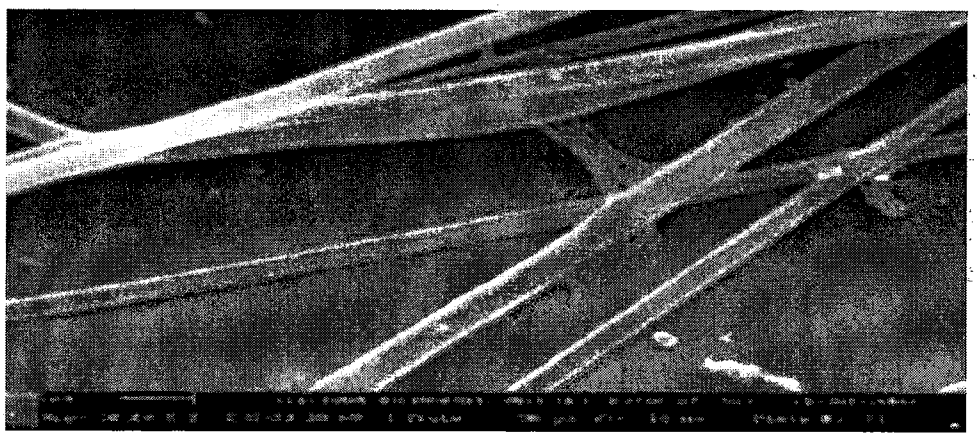

Figure 3.13. SEM image of PVA/AuNPs on fluorinated tin oxide.

Characterization of *Biotin-PEO-PS-PEO-Biotin.* The functional polymers were obtained in yields of 90% or higher as a white powder after precipitation into hexane. Table 3.5 lists the composition and molecular weights of polymers prepared by Scheme 3.2. The ^{1}HNMR of the tri-block copolymers are shown in Figure 3.14. In the NMR spectrum the peaksat 1.3 and 1.7 ppm are attributed to the CH and CH_2 protons of

polystyrene. The peaks at 7.0 and 6.5 ppm are credited to the aromatic protons in styrene. The sharp peak at 3.7 ppm is that of PEO.

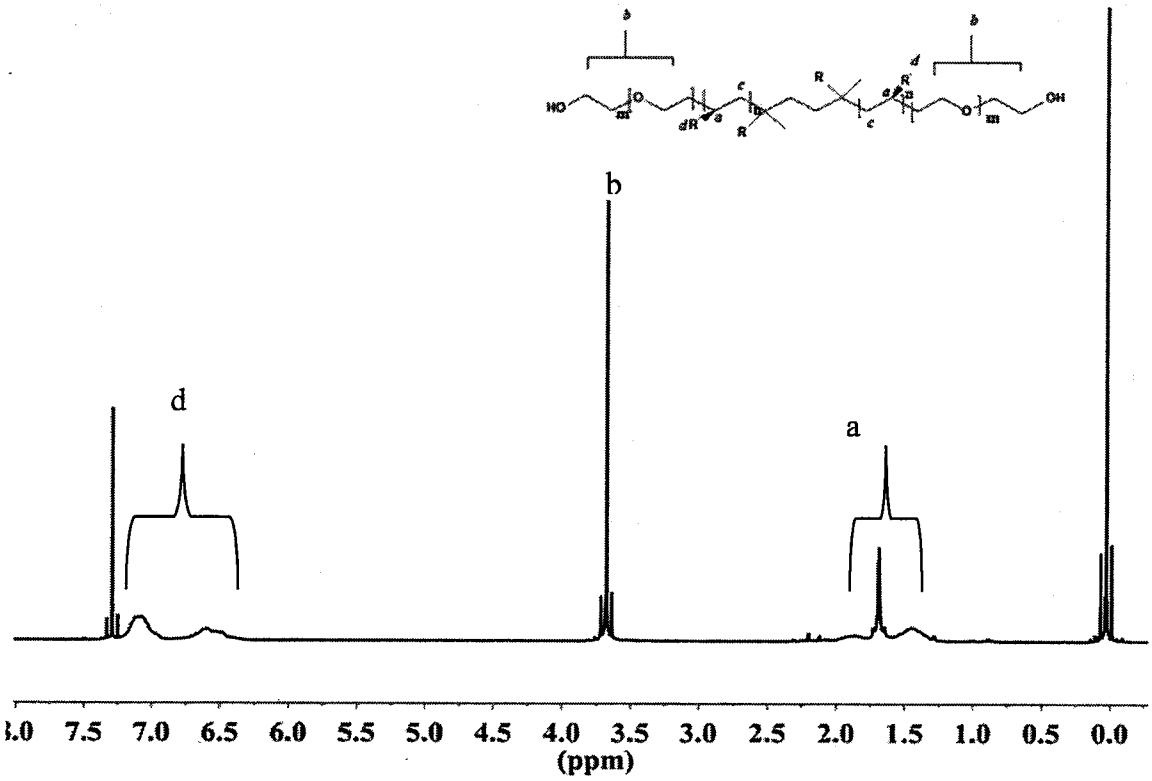

Figure 3.14. 500 MHz ^{1}HNMR of *HO-PEO-PS-PEO-OH* ran using $CDCl_3$ and tetramethylsilane as an internal standard.

FT-IR spectroscopy was used to determine the end functional groups before and after functionalization. Figure 3.15 shows the di-hydroxyl functional groups stretching at 3500 cm^{-1} for all of the polymers listed in Table 3.5 after termination with methanol. After coupling with biotin the hydroxyl group disappears, which is indicative of

quantitative functionalization. An amine stretching around 3400 cm^{-1} along with an ureido peak at 1600 cm^{-1} was observed after complete functionalization of the polymers. ^{1}HNMR was also used to determine the end functionalization of biotin at each chain end. Shown in Figure 3.16 is the spectrum of Biotin-PEO-PS-PEO-Biotin. At 4.3 (f) and 4.6 (g) ppm are attributed to the protons in biotin respectively.

Table 3.5. Composition and molecular weights of *α, ω-bi* [poly (ethylene oxide)-b-poly (styrene)-b-poly (ethylene oxide)]

Sample	M_1/M_2 (^{1}HNMR)	M_n (GPC)	M_w (GPC)	PDI	M_n (^{1}HNMR)
Sample 1	21/79	15k	20k	1.34	15k
Sample 2	21/79	18k	22k	1.24	13k
Sample 3	31/69	13k	25k	1.91	13k
Sample 4	32/68	-	-	-	33k

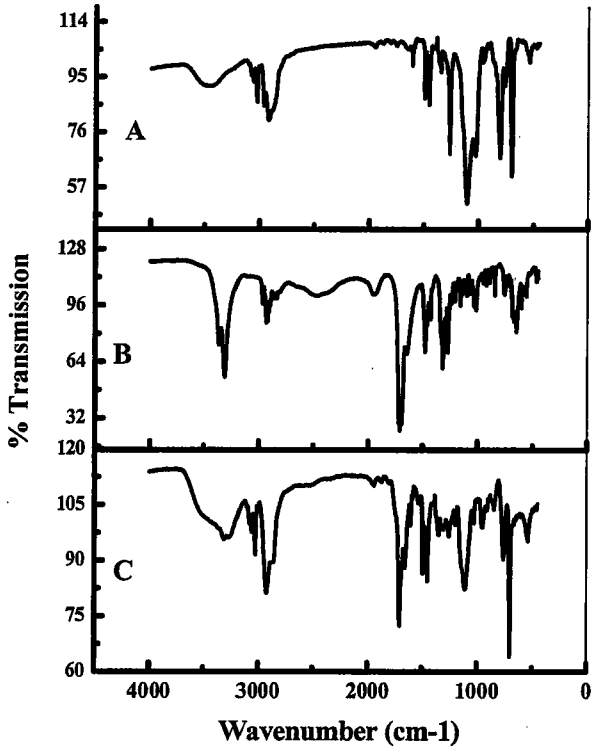

Figure 3.15. FT-IR of (a) *HO-PEO-PS-PEO-OH*, (b) Biotin and (c) *Biotin-PEO-PS-PEO-Biotin*

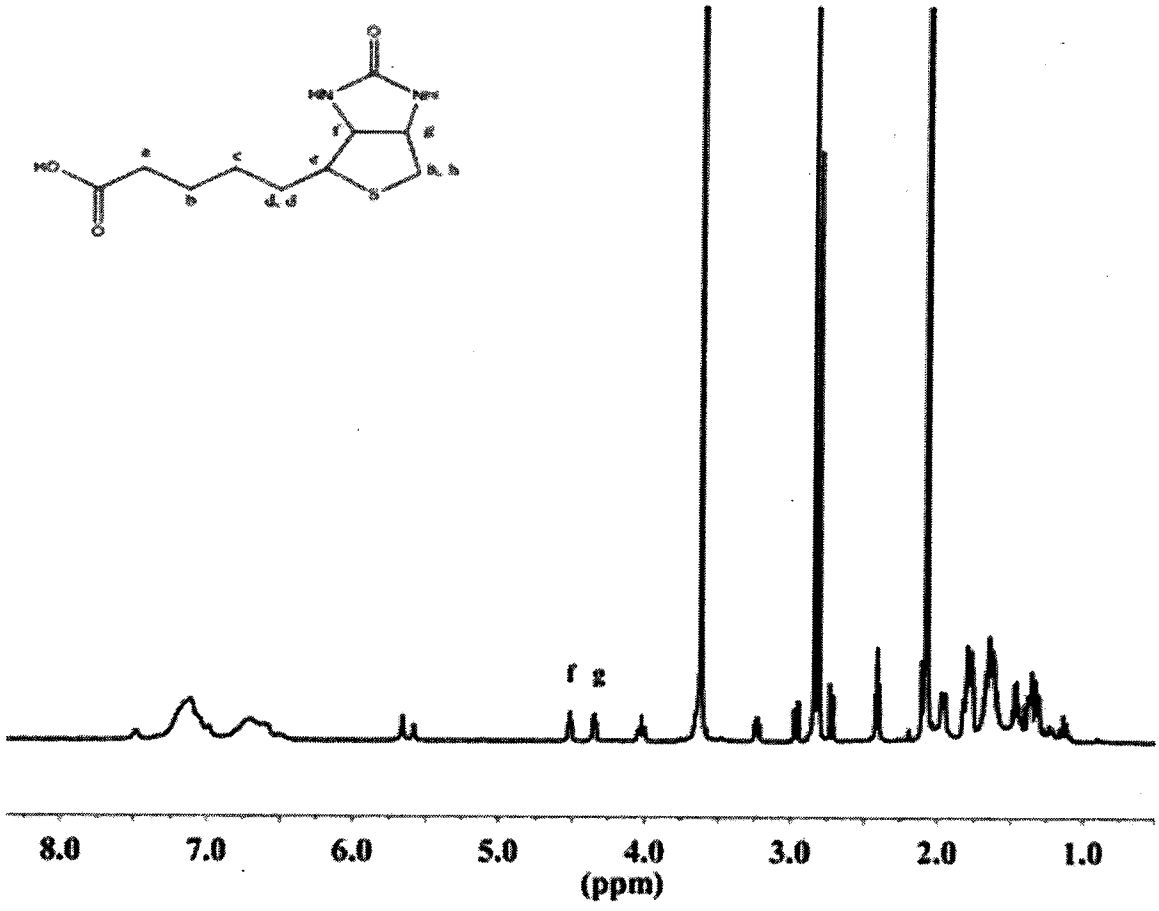

Figure 3.16. Spectrum of Biotin-PEO-PS-PEO-Biotin

The molecular weights of all polymers were determined using gel permeation chromatography (GPC) relative to polystyrene standards as shown in Figure 3.17. The molecular weights were determined using THF as the eluent as the polymers are soluble in this solvent. The lower molecular weight polymer distributions were slightly broad (1.3-1.9 kD). In contrast, the molecular weight distribution for higher polymers was narrow (1.24 kD) displaying a sharp peak.

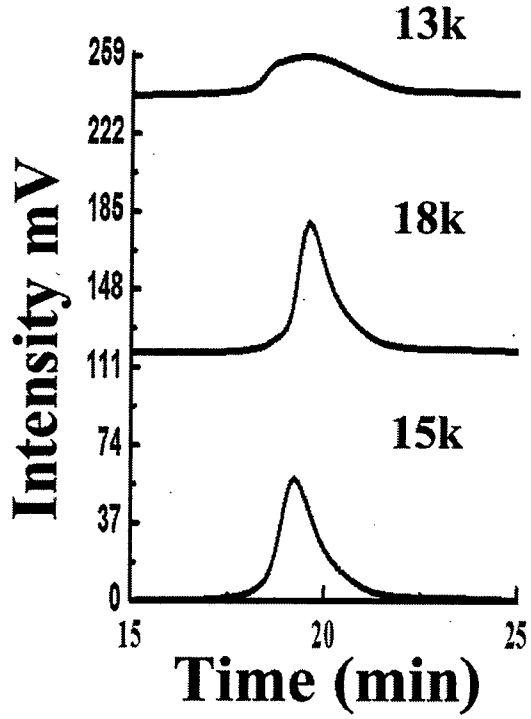

Figure 3.17. The molecular weights of 15, 18, and 13K samples determined by GPC.

To determine the thermal properties, differential scanning calorimetry (DSC) studies were carried out over the temperature range of 25 to 200°C. Figure 3.18 shows the DSC thermograms for the precursor polymer *OH-PEO-P2MS-PEO-OH* and after functionalization *Biotin-PEO-P2MS-PEO-Biotin* using 13K polystyrene from Table 3.5. All of the polymers exhibited a glass transition temperature around about 100°C which is attributed to the polystyrene block as shown in Table 3.6. However, there was no melting temperature present at 60°C for the PEO block, which indicates that the polystyrene microsphase is predominant. The functionalized polymers displayed a melting endotherm at 165°C, signifying the decomposition of biotin as the protein's melting temperature is around 233°C.

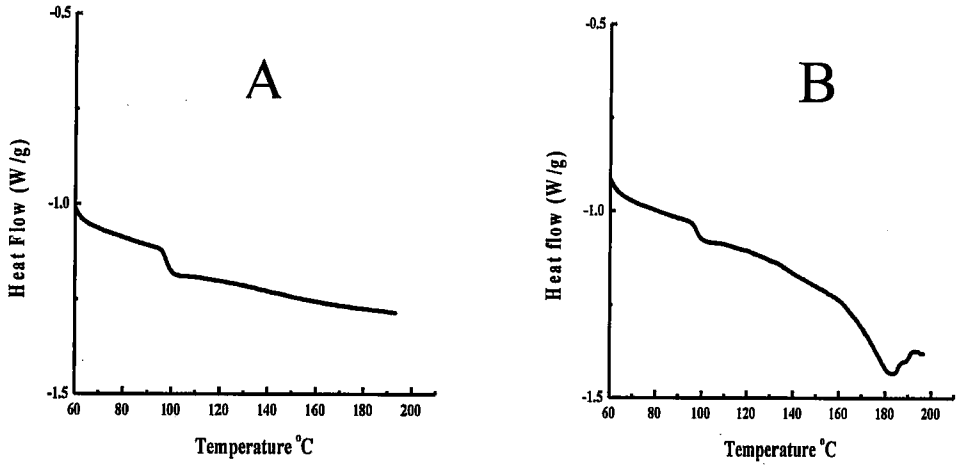

Figure 3.18. A. DSC of *OH-PEO-P2MS-PEO-OH* B. *Biotin-PEO-P2MS-PEO-Biotin*

The elemental composition of the OH-PEO-P2MS-PEO-OH fibers were analyzed using x-ray photoelectron spectroscopy (XPS) shown in table 3.6. The C1s and O1s signals appeared at 294 and 533 eV respectively. The carbon signal is accredited to the carbon backbone of PS and PEO. The Oxygenated species is due to the hydroxylated end groups of the tri-blocks. A Sn3d signal at 487 eV indicates that there's a slight contamination of tin on the fiber's surface. This contamination was less than 0.1 atom.% which is very insignificant (may arise from tin particles floating in the air). The presence of the AuNPs is evident in the survey scan in Figure 3.19 around 100 eV. The fibers diameters were measured using scanning electron microscopy (SEM) shown in Figure 3.20. The diameters were around 300 to 450 nanometers with a ropelike morphology.

Table 3.6. XPS measurements of fibers made using sample 3 and thiolated AuNPs

Samples	Atom	Peak (eV)	FWHM (eV)	Atom.%
13k AuNPs fibers	O1s	533.16	2.83	27.25
	Si2p	100.22	2.61	43.72
	C1s	294.08	3.28	25.01
	Sn3d	487.9	2.6	0.01

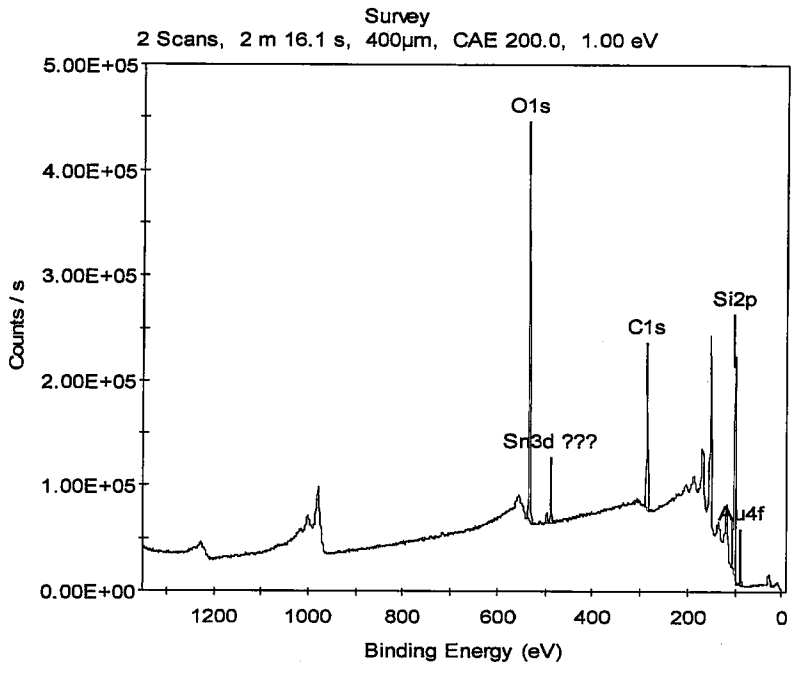

Figure 3.19. Survey scans of fibers comprised of 13K polystyrene with thiolated AuNPs.

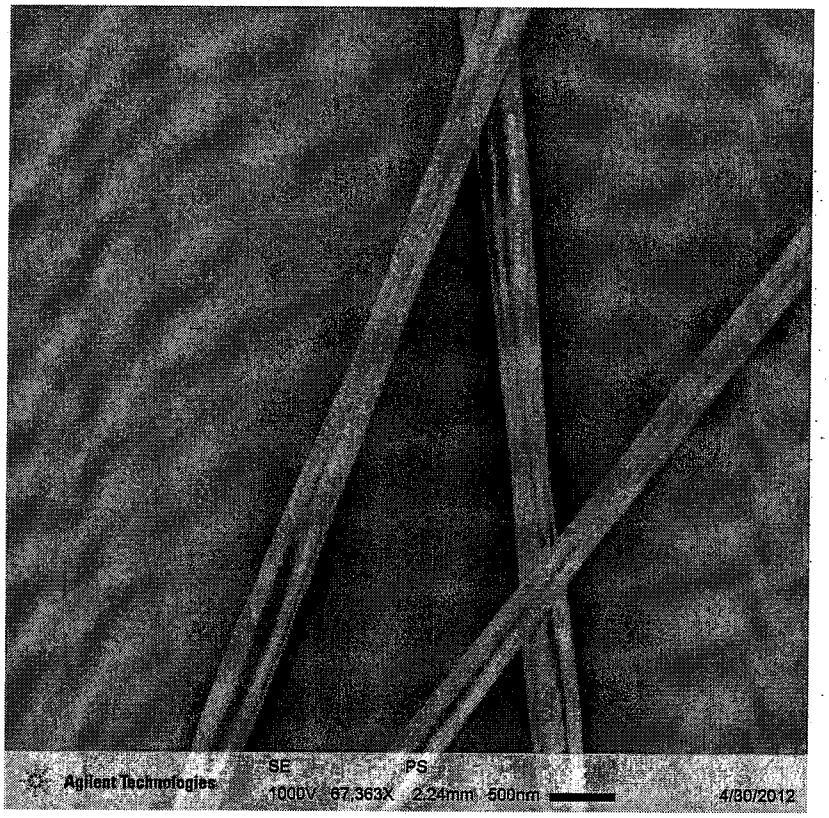

Figure 3.20. SEM Image of the nanofibers made using a 10 wt.% solution of the functional polymer and a high molecular weight PS in DMF.

CONCLUSION

Due to their enhanced physical and chemical properties paralleled to that of their counterparts, functional nanostructured materials have become a field of interests. Under the development of nanotechnology, nanostructured materials have garnered new properties and fabrication methods into the fabrication of new therapeutic tools and devices. However, the self-assembly of polymers constructs must be studied intently in order to achieve effective control over their propertied for the eventual fabrication of high performance devices.

Molecular assembly is ever-present in nature and in daily life. Hand washing, an everyday Hygienic routine, entails the self-assembly of soap bubbles from small molecules surfactant when soaps are used. While polymers are covalently constructed structures, block copolymers have the tendency to self-assemble into intricate higher ordered-structures via non-covalent interactions. Block copolymers such as rod-coil copolymers vary greatly from that of other block copolymer systems due to their inflexible chains structures, which leads to the adoption of extended rigid chain conformations.

The tailoring of these new technologies, results in a significant need to understand the mechanism in which one-dimensional nanostructures play a role in enhancing the mechanical and thermal properties of polymers. Block copolymers are ideal candidates for directing the assembly of nanoparticles into ordered structures. One-dimensional nanoparticles have been prepared by self-assembly of parent materials such as graphene. π-π Stacking usually dominates the self-assembly of these nanostructures because of delocalized π-electrons. This dissertation aims to understand the underlying process in

which phase transitions and surface effects occurs within polymer-particle composites in hopes of improving functional nanomaterials.

Nanomaterials are currently being used in the design of novel therapeutic agents for the use in FET sensors and other applications. These tools are aimed to replace long and arduous diagnostic processes such as ELISA for speedy pinpointing of diseases such as cancer, Alzheimer and cystic fibrosis to name a few. Point of care (POC) devices eliminate the need for ordering tests and sample transport leading to longer time prognosis. In this study, we aim to study the non-covalent interaction of nanoparticle-polymer formation and polymer-protein associations for the eventual development of novel straightforward biodiagnostic agents.

Role Of Polymer Stereoregularity On Nanocomposites Of Polystyrene With Single-Walled Carbon Nanotubes

Our results demonstrate that stereoregularity of polystyrene plays an important role in the formation of polystyrene/SWNT nanocomposites. Theoretical and experimental methods strongly suggest that the isotactic polystyrene is more effective in interacting with the SWNT compared to the atactic polystyrene. At low SWNT contents (< 1%), the SWNT is well dispersed within the isotactic polystyrene and forms a pseudo-crosslinked composite matrix. Due to the formation of the pseudo-crosslinked composite matrix, the glass transition temperature of the isotactic polymer composites increases with increasing SWNT content. The nanocomposite can be depicted as type-A matrix. On the other hand, even at low SWNT contents (< 1%), the atactic polystyrene/SWNT composite may be depicted by type-C matrix where the SWNT forms agglomerates since the interaction between the atactic polymer and SWNT is not as effective. Therefore, the

spatial orientation of the polymer repeating unit at the molecular level plays a significant role on the formation of polystyrene/SWNT nanocomposites.

Functional Polymer Nanostructures To Control Material-Cell Interactions

The most aligned nanostructures were prepared on silicon substrates using PVA and NPs made using the one-step method. The one-step technique reaction rate increased substantially after two-three hours where an increase in the absorption peak at 600 nm was observed via UV-vis. However, the fibers made with these nanoparticles agglomerated within the PVA matrix as shown in the TEM images. These agglomerations were as a result of not further functionalizing the particles with thiol groups. Using conductive substrates allowed the preparation of well-structured nanomaterials.

Functional polymer ligands of α, ω-bi[poly (ethylene oxide)-b-poly(styrene)-b-poly(ethylene oxide)], Biotin-PEO-PS-PEO-Biotin was prepared using living anionic polymerization, a synthetic method. The successful preparation and functionalization of these materials with biotin was evident in FTIR and NMR studies. The hydrophobic nature of these materials permitted the preparation and characterization of fibers using XPS and SEM for the eventual development of biosensors.

References

1. J.P. Billot, A. D., B. Gallot *Makromolekulare Chemie-Macromolecular Chemistry and Physics* **1976**, *177*, 1889.

2. B. Perly, A. D., B. Gallot *Makromolekulare Chemie-Macromolecular Chemistry and Physics* **1976**, *177*, 2569.

3. Shaw, A., Sriramula, S., S., Gosling, P.D., and Chryssanthopoulo, M.K. *Composites Part B* **2010**, *41*, 446.

4. O'Connell, M. J. *CRC Press: Boca Raton* **2006**.

5. Pozzo, D. C. W., L.M. *Eng. Aspects* **2007**, *294*, 117.

6. Jain, A. W., U. *Macromolecules* **2004**, *37*, 5665.

7. Cornil J, B. D., Calbert JP, Bredas JL *Adv. Mater.* **2001**, *13*, 1053.

8. Xia L, W. Z., Wan MX *J colloid Interf Sci* **2010**, *341*, 1.

9. Hangarter CM, B. M., Mulchandani A, Myung NV *J Material Chem* **2010**, *20*, 3131.

10. Arribart, H., Bensaude-Vincent, B. *Recherche* **1999**, *325*, 56.

11. Fujimasa, I. *Oxford University Press: Oxford* **1996**.

12. Kim, G.-M. W., A.; Radusch, H.-J.; Michler, G. H.; Simon, P.; Sperling, R. A.; Parak, W. J. *Chemistry of Materials* **2005**, *17*, 4949.

13. Jorge, P. M., Martins M.A., Trindade T., Santos J.L., Farahi F. *Sensors* **2007**, *7*, 3489.

14. Hezinger A .F. E., T. J., Gopferich A. *Eur. J. Pharm. Biopharm.* **2008**, *68*, 138.

15. Park H., Y. J., Seo S., Kim K., Suh J., Kim D., Haam S., Yoo K. H. *Small* **2008**, *4*, 192.

16. Couvreur, B. I. D. C. *Adv. Drug. Deliver. Rev.* **2002**, *54*, 631.

17. Boissiere M., A. J., Chaneac C., Brayner R., Devoisselle J. M., Livage J., Coradin T. *Int. J. Pharm.* **2007**, *344*, 128.

18. P., A. *Nat. Biotechnol.* **2004**, *22*, 47.

19. Asua J. M. *Polym. Sci.* **2002**, *27*, 1283.

20. Martins M.A., N. M. C., Esteves A. C. C.. Girginova P. I., Guiomar A. J., Amaral V. S., Trinadade T. *J. Mater. Chem.* **2008**, *18*, 4572.

21. Segalman, R. A. *Materials Science and Engineering R-Reports* **2005**, *48*, 191.

22. F.S. Bates, G. H. F. *Physics Today* **1999**, *52*, 32.

23. C. Harrison, J. A. D., D.H. Adamson *John Wiley & Sons Ltd., New York* **2004**, 295.

24. Olsen, B. D. S., R.A. *Materials Science and Engineering* **2008**, *62*, 37.

25. Ubblelohde A.R., L. L. A.; Oxford University Press, 1960.

26. Thompson T. E., F. E. R., Hanlon L.R. *Carbon* **1977**, *15*, 39.

27. Fuzellier H., M. J., Herold A. *Carbon* **1977**, *15*, 45.

28. Yan Q., H. B., Yu J., Wu J., et al. *Nano. Lett.* **2007**, *7*, 1469.

29. Shimizu T., H. J., Marcano D. C., Kosinkin D. V., Tour J. M., Hirose K. et al. *Nature Nanotechnol.* **2010**, *6*, 45.

30. Hu, Y. H. C., C. Y.; Wang, C. C. *Polym. Degrad. Stab* **2004**, *84*, 545.

31. Ash, B. J. S., L. S.; Siegel, R. W. *Mater. Lett.* **2002**, *55*, 83.

32. Ramanathan, T. A., A. A.; Stankovich, S.; Dikin, D. A.; Herrera-Alonso, M.; Piner, R. D.; Adamson D. H.; Schniepp, H. C.; Chen, X.; Ruoff, R. S.; Nguyen, S. T.; Aksay, I. A.; Prud'Homme, R. K.; Brinson, L. C. *Nature Nanotechnology* **2008**, *3*, 327.

33. Schniepp, H. C. e. a. *J. Phys. Chem. B* **2006**, *110*, 8535.

34. McAllister, M. J. e. a. *Chem. Mater.* **2007**, *19*, 4396.

35. Balazs A.C., E. T., Russel T.P. *Science* **2006**, *314*, 1107.

36. Dubertret B., S. P., Norris D.J., Noireaux V., Brivanlou A. H., Libchaber A. *Science* **2002**, *298*, 1759.

37. Lopes W.A., J. H. M. *Nature* **2001**, *414*, 735.

38. Oh M., M. C. A. *Nature* **2005**, *438*, 651.

39. Empedocles S., B. M. *Acc. Chem. Res.* **1999**, *32*, 389.

40. Clapp A. R., M. I. L., Mattoussi H. *ChemPhysChem* **2006**, *7*, 47.

41. Han M. Y., G. X. H., Su J. Z., Nie S. M. *Nat. Biotechnol.* **2001**, *19*, 631.

42. H., W. *Angew. Chem. Int. Ed* **1993**, *32*, 41.

43. Shenhar R., R. V. M. *Acc. Chem. Res.* **2003**, *36*, 549.

44. Zhang H., Z. C. C., Wang Y., Mohwald H. *Phys. Chem. Chem. Phys.* **2006**, *8*, 3288.

45. Lu C. L., G. C., Liu Y. F., Cheng Y. R., Yang B. *Chem. Mater.* **2005**, *17*, 2448.

46. Zhang H., Z. C. C., Wang Y., Zhang K., Ji X. L., Lu C. L., Yang B., Gao M. Y. *Adv. Mater.* **2003**, *15*, 777.

47. Lee J., S. V. C., Heine J. R., Bawendi M. G. Jensen K. F., *Adv. Mater.* **2000**, *12*, 1102.

48. Lee S. W., M. C. B., Flynn C. E., Belcher A. M. *Science* **2002**, *296*, 892.

49. Kazes M., L. D. Y., Ebenstein Y., Mokari T., Banin U. *Adv. Mater.* **2002**, *14*, 317.

50. Salguerino-MAceira V., C.-D. M. A. *Adv. Mater.* **2007**, *19*, 4131.

51. Rogach A. L., T. D. V., Shevchenko E. V. Kornowski A., Haase M., Weller H. *Adv. Funct. Mater.* **2002**, *12*, 653.

52. A., K. N. *MRS Bull.* **2001**, *26*, 992.

53. Tekin E., S. P. J., Hoeppner S., Van den Berg A. M. J., Susha A. S., Rogach A.L., Feldmann J., Schubert U.S. *Adv. Funct. Mater.* **2007**, *17*, 23.

54. Li M. J., Z. J. H., Zhang H., Liu Y. F., Wang C. L., Xu X., Tang Y., Yang B. *Adv. Funct. Mater.* **2007**, *17*, 3650.

55. Yang Y., H. J. M., Liu S. Y., Shen J.C. *J Material Chem* **1997**, *7*, 131.

56. Li D. X., C. Y., Wang K. W., He Q., Yan X. H., Li J. B. *Adv. Funct. Mater.* **2007**, *17*, 3134.

57. Kairdolf B. A., S. A. M., Nie S. M. *J. Am. Chem. Soc.* **2008**, *130*, 12866.

58. Edwards E. W., C. M., Wang D. Y., Mohwald H. *Angew. Chem. Int. Ed* **2008**, *47*, 320.

59. Shen Y., K. M., Shen Z., Nieberie J. Duan H.W., Frey H. *Angew. Chem. Int. Ed* **2008**, *47*, 320.

60. Leonov A. P., Z. J. W., Clogston J. D., Stern S. T., Patri A. K., Wei A. *ACS Nano* **2008**, *2*, 2481.

61 Kanaoka S., Y. N., Fukuyama Y., Aoshima S., Tsunoyama H., Tsukuda T., Sakurai H. *J. Am. Chem. Soc.* **2007**, *129*, 12060.

62. Sun L., C. R. M., Chechik V. *Chem. Commun.* **2001**, 359.

63. Sandros M. G., B. M., Maysinger D., Tabrizian M. *Adv. Funct. Mater.* **2007**, *17*, 3724.

64. Grady, B. P.; Paul, A.; Peters, J. E.; Ford, W. T. *Macromolecules* **2009**, *42*, 6152.

65. Mahdavian, A. R. S., Y.; Shaankareh, M *Polym. Bull.* **2009**, *63*, 329.

66. Pan, G. G., Q.; Tian, A.; He, Z. *Mater. Sci. Eng. A* **2008**, *492*, 383.

67. Hanemann, T. S., D. V. *Materials* **2010**, *3*, 3468.

68. Ziolo, R. F. G., E. P.; Shull, R. D. *Nanostruct. Mater.* **1993**, *3*, 85.

69. Gonsalves, K. E. C., X. H.; Baraton, M. I. *Nanostruct. Mater.* **1997**, *9*, 181.

70. Gupta S., Z. Q. L., Emrick T., Russell T. P. *Nano. Lett.* **2006**, *6*, 2066.

71. Ryan K. M., M. A., Stancil K. A., Liu H. T., Alivisatos A. P. *Nano. Lett.* **2006**, *6*, 1479.

72. Pang J. B., X. S. S., Jaeckel F., Sun Z. C., Dunphy D., Binker C. J. *J Am. Chem. Soc.* **2008**, *130*, 3284.

73. Khanal B. P., Z. E. R. *Angew. Chem. Int. Ed* **2007**, *46*, 2195.

74. Fava D., W. M. A., Kumacheva E. *Chem. Commun.* **2009**, 2571.

75. Nie Z. H., F. D., KumachevaE., Zou S., Walker G. C., Rubinstein M. *Nat. Material* **2007**, *6*, 609.

76. Gao M. Y., R. B., Kirstein S., Mohwald H. *J. Phys. Chem. B.* **1998**, *102*, 4096.

77. Ostrander J. W., M. A. A., Kotov N. A. *J. Am. Chem. Soc.* **2001**, *123*, 1101.

78. F., C. *Adv. Mater.* **2001**, *13*, 11.

79. Wang D. Y., R. A. L., Caruso F. *Nano. Lett.* **2002**, *2*, 857.

80. Gaponik N., R. I. L., Sukhorukov G. B., Weller H., Rogach A. L. *Adv. Mater.* **2002**, *14*, 879.

81. Sanchez-Gaytan B. L., C. W. H., Kim Y.,Mendez-Polanco M. A., Duncan T. V., Fryd M., Wayland B. B., Park S. J. *angew. Chem. Int. Ed* **2007**, *46*, 9235.

82. Jun Y. W., L. J. H., Cheon J. *Angew. Chem. Int. Ed* **2008**, *47*, 5122.

83. Chen Y. C., T. R., Snee P. T. *J. Am. Chem. Soc.* **2008**, *130*, 3744.

84. Lin C-. A. J., S. A., Li J. K., Yang T-. Y., Li P-. Y., Zanella M., Chang W. H., Parak W. J. *Small* **2008**, *4*, 334.

85. Kumar A., B. H. A., Whitesides G. M. *Langmuir* **1994**, *10*, 1498.

86. Ingrosso C., F. V., Stricolli M., Agostiano A., Voigt A., Gruetzner G., Curri M. L., Brugger J. *Adv. Funct. Mater.* **2007**, *17*, 2009.

87. Yin W., L. H., Yates M. Z., Du H., Jiang F., Guo L., Krauss T. D. *Chem. Mater.* **2007**, *19*, 2930.

88. Schlecht S. Tan S. T., Y. M., Dersch R., Wendorff J. H., Jia Z. H., Schaper A. *Chem. Mater.* **2005**, *17*, 809.

89. Zhang H., W. C. L., Li M. J., Zhang J. H., Yang B. *Adv. Mater.* **2005**, *17*, 853.

90. Huynh W. U., D. J. J., Alivisatos A. P. *Science* **2002**, *295*, 2425.

91. Dabbousi B. O., B. M. G., Onitsuka O., Rubner M. F. *Appl. Phys. Lett.* **1995**, *66*, 1316.

92. Robinson D. B., P. H. H. J., Zeng H., Li G. X., Pourmand N., Sun S. H., Wang S. X. *Langmuir* **2005**, *21*, 3096.

93. Kim B. S., Q. J. M., Wang J. P., Taton T. A. *Nano. Lett.* **2005**, 1987.

94. Zhang H., H. J., Yang B. *Adv. Funct. Mater.* **2010**, *20*, 1533.

95. Yang J, D. S. R. G. X. H. *J Am. Chem. Soc.* **2008**, *130*, 5286.

96. G., D. *Science* **1997**, *277*, 1232.

97. Mamendov A. A., B. A., Giersig N., Mamedova N. N., Kotov N. A. *J Am. Chem. Soc.* **2001**, *123*, 7738.

98. Crisp M. T., K. N. A. *Nano. Lett.* **2003**, *3*, 173.

99. al., G. O. e. *Nat. Med.* **2003**, *9*, 104.

100. al., A. L. e. *Chem. Soc. Rev.* **2011**, *40*, 860.

101. al., L. J. D. C. e. *Angew. Chem. Int. Ed* **2010**, *49*, 6954.

102. al., H. K. e. *Angew. Chem.* **2011**, *123*, 3073.

103. al., J. K. e. *J. Am. Chem. Soc.* **2000**, *122*, 540.

104. al., T. W. e. *Nat. Biotechnol.* **1997**, *15*, 358.

105. Rauwald U., S. O. A. *Angew. Chem. Int. Ed* **2008**, *47*, 3950.

106. Coulston R. J.. Jones S. T., L. T.-C., Appel E.A., Scherman O. A. *Chem. Commun. (Camb.)* **2011**, *47*, 164.

107. Patil A., S. I. M., Kadam V.J., Jadhav K.R. *Curr. Nanosci.* **2009**, *5*, 141.

108. P., D. *Curr. Pharm. DEs.* **2009**, *15*, 153.

109. Greco F., V. M. J. *Front. Biosci.* **2008**, *13*, 2744.

110. Riehemann K., S. S. W., Luger T.A., Godin B., Ferrari M., Fuchs H. *Angew. Chem.* **2009**, *121*, 872.

111. Miller K., S.-F. R. *Wiley Encyclopedia of Chemical Biology*; Wiley Inter-Science: Hoboken, 2009; Vol. 3.

112. Duncan R., R. H., Satchi-Fainaro R. *J. Drug Targeting* **2006**, *14*, 337.

113. Orive G., H. R. M., Gascon R.A., Dominguez-Gil A., Pedraz L. J. *Curr. Opin. Biotechnol* **2003**, *14*, 659.

114. Salmaso S., B. S., Semenzato A., Caliceti P. *J. Nanosci. Nanotechnol.* **2006**, *6*, 2736.

115. Caliceti P., V. F. M. *Adv. Drug. Deliver. Rev.* **2003**, *55*, 1261.

116. Bilati U., A. E., Doelker E. *Drug Delivery Technol.* **2005**, *5*, 42.

117. Veronese F. M., C. P., Schiavon O., Sergi M. *Adv. Drug Delivery Rev* **2002**, *52*, 97.

118. Matsumara Y., M. H. *Cancer Res.* **1986**, *46*, 6387.

119. Bowen S., T. N., Inoue T., Yamasaki M., Okabe M., Horri I., Eliason J. F., *Exp. Hematol.* **1999**, *27*, 425.

120. Veronese F. M., C. P. *Cancer Drug Delivery and Development: Tumour Targeting in Cancer Thearpy*; Humana Press: New York, 2005.

121. Caliceti P., M. M., Schiavon O., Sartore L., Monfardini C., Veronese F.M. *J. Bioact. Compat. Polym.* **1993**, *8*, 41.

122. Caliceti P., M. M., Schiavon O. Monfardini C., Veronese F.M. *Bioact. Compat. Polym.* **1994**, *9*, 252.

123. Salmaso S., B. S., Scomparin A., Mastrotto F., Caliceti P. *Isr. J. Chem* **2010**, *50*, 160.

124. Piedmonte D.M., T. M. J. *Adv. Drug Delivery Rev* **2008**, *60*, 50.

125. Roberts M. J., B. M. D., Harris J. M. *Adv. Drug Delivery Rev* **2002**, *54*, 459.

126. Brocchini S., G. A. B. S., Choi J., Zloh M., Shaunak S. *Adv. Drug Delivery Rev* **2008**, *60*, 3.

127. Tirat A., F. T., Stettler T., Mayr L. M., Leder L.E. *Int. J. Biol. Macromol.* **2006**, *39*, 66.

128. Deiters A., C. T. A., Summerer D., Mukherji M., Schultz P. G. *Bioorg. Med. Chem. Lett.* **2004**, *14*, 5743.

129. DeFrees S., W. Z. G., Xing R., Scott A.E., Wang J., Zopf D., Gouty D.L., Sjoberg E. R., Panneerselvam K., Brinkman-Van der Linden, Bayer R. J., Tarp M. A., Clausen H. *Glycobiology* **2006**, *16*, 833.

130. Salmaso S., B. S., Semenzato A., Matstroto F., Scomparin A., Caliceti P. *Eur. Polym. J.* **2008**, *44*, 1378.

131. King T. P., Z. S. W., Lam T. *Biochemistry* **1986**, *25*, 5774.

132. Sawant S. M., H. J. P., Salmaso S., Kale A., Tolcheva E., Levchenko T. S., Torchilin V. P. *Bioconjugate Chem.* **2006**, *17*, 943.

133. Ladue, J. S., F. Wroblewski and A. Karmen *Science* **1954**, *120*, 497.

134. Cui, Y., Q.Q Wei, H.K. Park, C.M. Lieber *Science* **2001**, *293*, 1289.

135. Chua, J., R.E. Chee, A. Agarwal, S.M. Wong and G. J. Zhang *Anal. Chem.* **2009**, *81*, 6266.

136. Bunimovich, Y. L., Y.S. Shin, W.S. Yeo, M. Amori, G. Kwong and J.R. Heath *J. Am. Chem. Soc.* **2006**, *128*, 16323.

137. Patolsky, F., G. Zheng, O. Hayden, M. Lakadamyali, X. Zhuang and C.M. Lieber *Proc. Natl. Acad. Sci. USA* **2004**, *101*, 14017.

138. Lu, W. C. M. L. *J. Phys. D: Appl. Phys.* **2006**, *39*, R387.

139. Zhang, G. J., Zhang, M.J. Huang, Z.H.H. Luo, G.K.I. Tay, E.J.A. Lim, T.G. Kang, Y. Chen *Sens. Actuators B: Chem.* **2010a**, *146*, 138.

140. Zheng, G., F. Patlosky, Y. Cui, W.U. Wang, C.M. Lieber *Nat. Biotechnol.* **2005**, *23*, 1294.

141. Chen R J, Z. Y., Wang D, Dai H *J. Am. Chem. Soc.* **2001**, *123*, 3838.

142. E, S. *J. Mammary Gland Biol. Neoplasia* **2000**, *5*, 95.

143. E, S. *Oncogene* **2003**, *22*, 6589.

144. Sachdev D, Y. D. *Endocr. Relat. Cancer* **2001**, *8*, 197.

145. M, P. *Recent Results Cancer Res.* **1998**, *152*.

146. Shao N, L. S., Wickstrom E, Panchapakesan B *Nanotechnology* **2007**, *18*, 315101.

147. Shao N, L. S., Wickstrom E, Panchapakesan B *Nanotechnology* **2008**, *19*, 465101.

148. HedbergJ, D. L., Jiao J *Appl, Phys. Lett.* **2005**, *86*.

149. Lay M.D., N. J. P. S. E. S. *Nano. Lett.* **2004**, *4*, 603.

150. Bradley K, B. M., Star A, Gruner G. *Nano. Lett.* **2004**, *4*, 253.

151. Heller I, J. A. M., Mannik J, Minot E.D., Lemay S.G. Dekker C *Nano. Lett.* **2008**, *8*, 591.

152. Wu G, D. R. H., Hansen K.M., Thundat T, Cote R. J., Majumdar A *Nat. Biotechnol.* **2001**, *19*, 856.

153. al, W. G. e. *Proc. Natl. Acad. Sci. USA* **2001**, *98*, 1560.

154. Fritz J, B. M. K., Lang H.P., Rothuizen H, Vettiger P, Meyer E, Guntherodt H -J, Gerber Ch, Gimzewski J.K. *Nanomechanics Science* **2000**, *288*, 316.

155. Kim, H.; Abdala, A. A.; Macosk, C. W. *Macromolecules* **2010**, *43*, 6515–6530.

156. Vaia, R. A.; Maguire, J. F. *Chem. Mater.* **2007**, *19*, 2736-2751.

157. Benmouna, R.; Benmouna, M. *J. Chem. Eng. Data* **2010**, *55*, 1759-1767.

158. Chen, K.; Harris, K.; Vyazovkin, S. *Macromol. Chem. Phys.* **2007**, *208*, 2525-2532.

159. Eckman, R. R.; Henrichs, P. M.; Peacock, A. J. *J. Macromolecules* **1997**, *30*, 2474-2481.

160. Tchoul, M. N.; Ford, W. T.; Ha, M. L. P.; Chavez-Sumarriva, I.; Grady, B. P.; Lolli, G.; Resasco, D. E.; Arepalli, S. *Chem. Mater.* **2008**, *20*, 3120-3126.

161. Smith, G. D.; Bedrov. D. *Langmuir* **2009**, *25*, 11239-11243.

162. Pandey, Y. N.; Papakonstantopoulus, G. J.; Doxastakis, M. *Macromolecules* **2013**, *46*, 5097-5106.

164. Szleifer, I.; Yerushalmi-Rozen, R. *Polymer* **2005**, *46*, 7803-7818.

165. Bikiaris, D. *Materials* **2010**, *3*, 2884-2946.

166. Alig, I.; Lellinger, D.; Engel, M.; Skipa, T.; Potschke, P. *Polymer* **2008**, *49*, 1902-1909.

167. Shaw, A.; Sriramula, S.; Gosling, P. D.; Chryssanthopoulo, M. K. *Composites Part B* **2010,** *41*, 446-453.

168. Guenet, J. M.; Picot, C.; Benoit, H. *Macromolecules* **1979**, *12*, 86-90.

169. Atkins, E. D. T.; Keller, A.; Shapiro, J. S.; Lemstra, P. J. *Polymer* **1981**, *22*, 1161-1164.

170. Nakaoki, T.; Kobayashi, M. J. *J. Mol. Struct.* **2003**, *655*, 343-349.

171. Shammgharaj, A. M.; Bae, J. H.; Nayak, R. R.; Ryu, S. H. *J. Polym. Sci. Part A: Polym. Chem.* **2007**, *45*, 460-470.

172. Stevens, M. P. *Polymer Chemistry: An Introduction.* 3rd Ed.; Oxford University Press: New York, **1998.**

173. Hanemann, T.; Szabo, D. V. *Materials* **2010**, *3*, 3468-3517.

174. Grady, B. P.; Paul, A.; Peters, J. E.; Ford, W. T. *Macromolecules* **2009**, *42*, 6152-6158.

175. Sundararajan, P. R.; Tyrer, N. *Polymer* **1981**, *6*, 359-366.

176. Tchoul, M. N.; Ford, W. T.; Lolli, G.; Resasco, D. E.; Arepalli, S. *Chem. Mater.* **2007**, *19*, 5765–5772.

177. Materials Studio, *Accelrys Material Studio*, 5.5; Accelrys Software Inc.: San Diego, CA.

178. Huang, C.-L.; Chen, Y.-C.; Hsiao, T.-J.; Tsai, J.-C.; Wang, C. *Macromolecules* **2011**, *44*, 6155-6161.

179. Bovey, F. A.; Mirau, P. *NMR of Polymers*. 1st Ed.; Elsevier Science and Technology, **1996**.

180. Grossiord, N.; Miltner H. E.; Loos, J.; Meuldijk, J.; Mele, B. V.; Koning, C. E. *Chem Mater.* **2007**, *19*, 3787 -3792.

181. Li, J.; Khan, I. M. *Macromolecules* **1993**, *26*, 4544-4550.

182. Li, J; Pratt, L. M.; Khan, I. M. *J. Polym. Sci. Poly Chem. Ed.* **1995**, 33, 1657-1663.

183. Powell, E.; Lee, Y-H; Partch, R.; Dennis, D.; Moreg, T.; Varshney, M. *Int. J. Nanomedicine* **2007**, *3*, 449-459.

184. Reuven, D.; Suggs, K.; Wiliams, M. D.; Wang, X. Q. Acs Nano 2012, 6, 1011-1017.

185. Marek, M.; Kaiser, K.; Gruber, H. J. *Bioconjug Chem* **1997** 580-586.

186 Patil, Y.; Toti, U.; Khadir, A.; Ma, L. Panyam, J. Biomaterials **2009**, 30 459-866.

187 Kiessling, L. L; Gestwicki, J. E.; Strong, L. E. *Angew Chem. Int.* **2006** Ed. 45 2348-2368.

188. Mammen, M.; Choi, S. K.; Whitesides, G. M. *Angew Chem. Int.* **1998** Ed. 37 2754-2794.

189. Veronese, F. M.; Morpurgo, M. *Farmaco* **1999**, 54, 497-516.

190. Weiss, A.; Littman, D. R. *Cell* **1994** 76 263-274.

191. El Fray, M.; Prowans, P.; Puskas, J. E., Altstads, V. *Biomacromolecules* **2006**, 7, 844-850.

192. Baeumner, A. J. *Analytical and Bioanalytical Chemistry* **2003**, 377, 434-445.

193. Edwards, K. A.; Clancy, H.A; Baeumner, A. J. *Analytical and Bioanalytical Chemistry* **2006**, 121, 158-177.

194. Pereira, A. S.; Daniel-da-Silva, A. L.; Trindade, T. *From Nanoparticles to Nanocomposites: a Brief Overview* **2011**.

195. Liu, S.; Chen, G.; Prasad, P. N.; Swihart, M.T. *Chemistry of Materials* **2011**, 23, 4098-4101.

196. Kastner, M. A. *Phys. Today* **1993**, 46, 24.

197. Lewis, L. N. *Chem. Rev.* **1993**, 258-414.

198. Szwarc, M. Wiley, New York **1968**.

ABSTRACT

DEPARTMENT OF CHEMISTRY

LONDON, LAURISA A. B.S. CLARK ATLANTA UNIVERSITY, 2008

THE EFFECT OF STEREOCHEMISTRY AND CONFORMATION ON NANOCOMPOSITE FORMATION

Committee Chair: Ishrat Khan, Ph.D.

Dissertation dated December 2013

Through the dispersion of nanofillers into polymer matrices, high-performance lightweight composites were heralded as the new class of materials with multifunctional properties. Although the design and fabrication of nanocomposites with flexible and controlled properties are an ongoing challenge, these materials have potential use in microoptics, electronics and solar cells. Nanofillers enhanced performance is achieved by their inherent optical, electrical and magnetic properties. These properties become more evident with decreasing particle size, thus leading to an increase in the surface/volume ratio. The filler's properties at a nano-scale are substantially different compared to that of their bulk counterparts. Therefore, the smaller a particle is, the greater its role in influencing the interfacial and physical properties as well as agglomeration behavior of composites. While much is known about polymer material preparation, not much is

understood on how to tailor polymer structures to control self-assembly. With the pioneering of new technologies there is still a great desire to fully understand the mechanism by which one-dimensional nanostructures change the structural and thermal properties of host materials. In order to fabricate high performance devices, it is crucial to achieve effective control over the self-assembly of copolymers and their fillers. Understanding the process, phase transitions, and surface effects in which particle-polymer interact is important in developing a broader perspective on composite formation.